



FACULTY OF SCIENCE AND TECHNOLOGY

MASTER THESIS

Study programme / specialisation:

MSc in Marine and Offshore Technology

The spring semester, 2022

Author: Martin Sande Lervik

Open / Confidential

Martin Sande Lervik

(signature author)

Course coordinator: Professor Yihan Xing

Supervisor(s):

Associate Professor Lin Li

Doctor Xinying Zhu

Thesis title:

Numerical analysis and risk analysis of the lifting operation of a subsea template

Credits (ECTS):

30

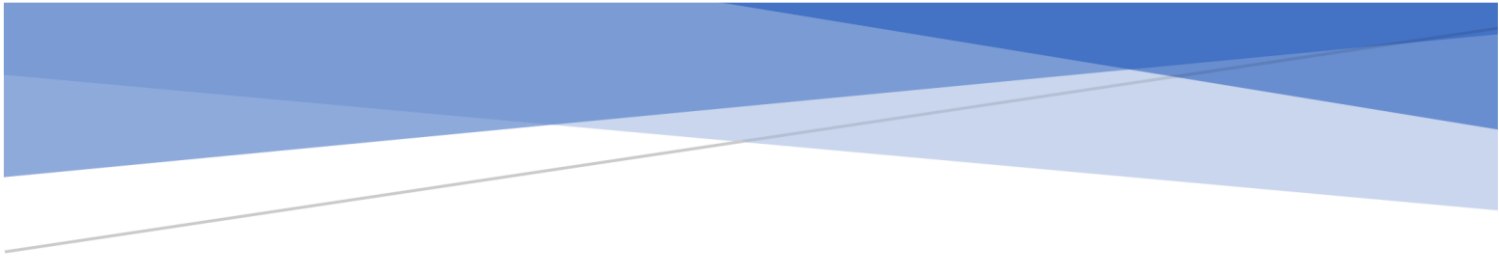
Keywords:

Marine lifting operation, splash-zone crossing, suction-anchor geometry, risk analysis, HAZOP

Pages: *57*

+ appendix: *10*

Stavanger, June 15, 2022



NUMERICAL ANALYSIS AND RISK ANALYSIS OF THE LIFTING OPERATION OF A SUBSEA TEMPLATE

Author: Martin Sande Lervik
Supervisor: Assoc. Prof. Lin Li
Co-supervisor: Dr. Xinying Zhu

University of Stavanger
Faculty of Science and Technology
Department of Mechanical and Structural Engineering and Material Science
Master's Thesis
Spring 2022

Abstract

Two different templates, template A and template B, for subsea oil and gas production are studied in this work. Numerical time-domain simulations for the crossing of the splash zone are run in OrcaFlex. Template A has suction anchors that have a diameter of 6 m and a height of 7.9 m, while template B's suction anchors have a diameter of 5.5 m and a height of 8.225 m. This thesis presents the numerical model and setup of the system, as well as the results of the simulations. The significant wave height was set to 2 m, the wave direction to 165 degrees and the following mean zero up-crossing periods were used: 4 s, 6 s, 8 s and 10 s. The results showed that the Gumbel probability paper for template A, with a mean zero up-crossing periods of 4 s, did not satisfy the 95 % probability of non-exceedance. It was also noted that the dynamic response decreased with increasing mean zero up-crossing periods. In conclusion, template A caused generally higher tension in the lifting wire, which may be attributed to the higher added mass.

Additionally, a HAZOP study is performed for the lifting operation. The hazards for the four phases lift-off and in-air manoeuvring, splash-zone crossing, deeply submerged, and landing, are identified and assessed. It was found that excessive tension, loads and motion were causing the majority of the hazards in the lift-off- and in-air-manoeuving phase and the splash-zone-crossing phase. Therefore, the two first phases of a marine lifting operation depend on the weather conditions to a great extent. The deeply-submerged phase and the landing phase involve a high number of potential threats. Misalignment with the production system is a detrimental consequence. The operation must be carefully planned and coordinated.

Acknowledgement

My supervisor, Assoc. Prof. Lin Li, has been incredibly helpful and encouraging throughout my work. She has accepted all of my requests for assistance and guidance. I would also like to thank her for her patience and kindness, which have undoubtedly helped me complete this project. Despite her busy schedule, I always felt welcome in her office.

Moreover, I am grateful for the guidance and technical explanations my co-supervisor Dr. Xinying Zhu provided. I gained a much better understanding of the topic thanks to her.

I would also like to thank my friends and fellow students Aslak Tjølsen, Vegard Reisæter, Fredrik Hovden Undstad and Pawel Klis for their valuable advice, suggestions, and discussions. Their knowledge and background from the aquaculture industry, well-intervention operations, offshore installations, and subsea technology have been beneficial.

The various tasks that were accomplished regarding the risk analysis in this project would not have been possible without the help and advice of Åge Tjelta Landråk, who has over 30 years of experience in the industry.

Lastly, I would like to thank my wife, Monika, for her patience and support throughout my studies. Her encouragement and inspiration have been crucial to me. She is truly irreplaceable.

Martin Sande Lervik
June 2022
Stavanger

Abbreviations

ALARP	As low as reasonably practicable
CCS	Carbon capture and storage
CDF	Cumulative distribution function
DoF	Degree of freedom
DS	Deeply submerged
FAR	Fatal accident rate
HAZID	Hazard identification
HAZOP	Hazard and operability
HSE	Health, safety and environment
ILS	Inline structure
IPCC	Intergovernmental panel on climate change
ITS	Integrated template structure
JONSWAP	Joint North Sea Wave Project
LG	Landing
LO	Lift-off and in-air manoeuvring
NCS	Norwegian continental shelf
o.e.	Oil equivalents
PLEM	Pipeline end module/manifold
PLET	Pipeline end termination
PSA	Petroleum Safety Authority Norway
RAO	Response amplitude operator
ROV	Remotely operated vehicle
SC	Splash-zone crossing
SPS	Subsea production system

Table of Contents

1	Introduction	1
1.1	Background and motivation.....	1
1.1.1	Norwegian oil and gas industry.....	1
1.1.2	Historical background	1
1.1.3	Future trends	3
1.2	Subsea structures and equipment.....	4
1.2.1	Pipeline end terminations.....	5
1.2.2	Jumpers.....	5
1.2.3	Subsea wellheads and Christmas trees.....	5
1.2.4	Manifold.....	6
1.2.5	Integrated template structure	6
1.3	Marine crane-lifting operation	7
1.3.1	Lift-off and in-air manoeuvring.....	7
1.3.2	Splash-zone crossing	7
1.3.3	Deeply submerged	7
1.3.4	Landing.....	7
1.4	Objective	7
1.5	Thesis structure.....	8
2	Theory	9
2.1	Waves.....	9
2.1.1	Irrotational flow	9
2.1.2	Wave spectrum	11
2.2	Vessel motion.....	12
2.2.1	Crane-tip motion.....	12
2.3	Dynamic loads for splash-zone crossing	13
2.3.1	Added-mass coefficient	14
2.3.2	Slamming force	14
2.3.3	Drag coefficient.....	15
2.4	Weather	15
2.5	Probability.....	15
2.5.1	Gumbel distribution	15
3	Numerical model.....	17
3.1	OrcaWave.....	17
3.2	Template models	18
3.3	Hydrodynamic forces	19

3.3.1	Added mass.....	19
3.3.2	Slamming.....	23
3.3.3	Drag.....	23
3.4	Environmental data.....	23
3.5	Crane and lifting wire.....	24
3.6	Duration and stages.....	25
4	Operational criteria.....	26
5	Results and discussion.....	27
5.1	Time history of tension.....	27
5.2	Gumbel probability paper.....	29
6	Risk assessment.....	33
6.1	Risk acceptance criteria.....	33
6.2	ALARP.....	34
6.3	The risk assessment process.....	35
6.4	HAZOP studies.....	38
7	Conclusions and further work.....	45
7.1	Numerical analysis conclusion.....	45
7.2	Risk analysis conclusion.....	45
7.3	Recommendations for future work.....	45
8	References.....	46
9	Appendix A: Spreadsheet containing calculation of hydrodynamic coefficients.....	50
9.1	Template A.....	50
9.2	Template B.....	53
10	Appendix B: MATLAB code for post-processing of results.....	58

List of Figures

Fig. 1.1. Production forecast in Norway, given in oil equivalents (o.e.). Adapted from [5]	1
Fig. 1.2. The Ormen Lange gas field in the Norwegian Sea. Adapted from [8].....	2
Fig. 1.3. Subsea Christmas tree. Adapted from [12].....	3
Fig. 1.4. Field layout of the Who Dat field in the Gulf of Mexico. Adapted from [21].....	5
Fig. 1.5. ITS structure for the Maria subsea field in the Norwegian Sea. Adapted from [23].....	6
Fig. 2.1. The six degrees of freedom of a vessel. Adapted from [33]	12
Fig. 2.2. The shielding effect. Adapted from [35]	13
Fig. 3.1. OrcaWave model.....	17
Fig. 3.2. Vessel displacement RAO from OrcaFlex.	18
Fig. 3.3. Analytical added-mass coefficient. Adapted from [27].....	19
Fig. 3.4. Components of the axial added mass for the suction anchors.	20
Fig. 3.5. OrcaFlex suction-anchor model with line elements representing added mass.....	20
Fig. 3.6. Vertical added-mass coefficient and its derivative of a cylinder of radius r . Adapted from [27]	21
Fig. 3.7. Normalised submergence. Adapted from [27].....	21
Fig. 3.8. Wave direction.	24
Fig. 5.1. Lifting-wire tension for template A for still water and for $T_z = 4$ s.....	27
Fig. 5.2. Lifting-wire tension for template A for $T_z = 6$ s for two different seeds.	28
Fig. 5.3. Lifting-wire tension for template A and B for $T_z = 4$ s for same seed.	29
Fig. 5.4. Gumbel probability paper for template A and B for $T_z = 4$ s.....	30
Fig. 5.5. Gumbel probability paper for template A and B for $T_z = 6$ s.....	31
Fig. 5.6. Gumbel probability paper for template A and B for $T_z = 8$ s.....	31
Fig. 5.7. Gumbel probability paper for template A and B for $T_z = 10$ s.....	32
Fig. 6.1. The ALARP principle. Adapted from [53].....	34
Fig. 6.2. Risk assessment process. Adopted from [54]	35
Fig. 6.3. HAZOP guide words. Adapted from [58].....	38

List of Tables

Table 3.1. Template specifications.....	18
Table 3.2. Data points generated from Figure 3-5 in [27].	22
Table 3.3. Environmental data.....	24
Table 3.4. Coordinates of crane tip.....	24
Table 3.5. Simulation stages.	25
Table 4.1. Upper load limit for the lifting-wire tension.	26
Table 4.2. Lower load limit for the lifting-wire tension.	26
Table 6.1. Risk matrix.....	36
Table 6.2. Risk limits.....	36
Table 6.3. Impact description.	37
Table 6.4 HAZOP study of the lift-off and in-air-manoeuving phase.	40
Table 6.5. HAZOP study of the splash-zone-crossing phase.	41
Table 6.6. HAZOP study of the deeply-submerged phase.	42
Table 6.7. HAZOP study of the landing phase.....	43

1 Introduction

1.1 Background and motivation

1.1.1 Norwegian oil and gas industry

Norway's petroleum industry is the largest source of revenue for the state, and it has been instrumental in developing the country's welfare state. Its value creation and revenues have helped make Norway one of the wealthiest nations in the world. In addition to being the dominant domestic industry, Norwegian gas export ensures energy security on the European continent [1, 2]. The historical and forecasted production in Norway can be seen in Fig. 1.1.

The recovery from the Covid-19 pandemic is expected to boost the global energy demand to 2019 levels and beyond, according to the Global Energy Review 2021 by the International Energy Agency [3]. Fossil fuels are an essential energy source and will most likely remain a substantial part of the energy supply until the 2030s, if not further into the future [4]. Taking the present energy-supply situation in Europe into consideration, it could be argued that the oil and gas production should be increased.

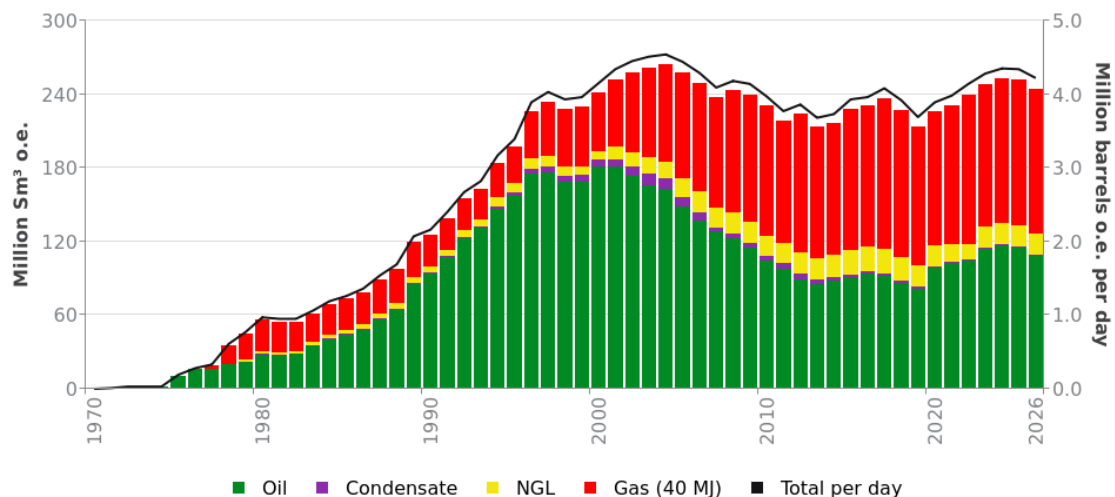


Fig. 1.1. Production forecast in Norway, given in oil equivalents (o.e.). Adapted from [5]

1.1.2 Historical background

The World's first offshore well was completed in 1947 in the Gulf of Mexico off the coast of Louisiana by Kerr-McGee Oil Industries. Although there had previously been produced oil and gas from wells under water, they were close to shore in relatively calm waters [6]. In 1961, Shell completed what is considered the first subsea well in the Gulf of Mexico. Many oil companies followed suit and subsea solutions proved to be cost-effective and safe [7]. Today, fields may be developed without topside facilities because the field can be tied back to shore, like the Ormen Lange field (Fig. 1.2).

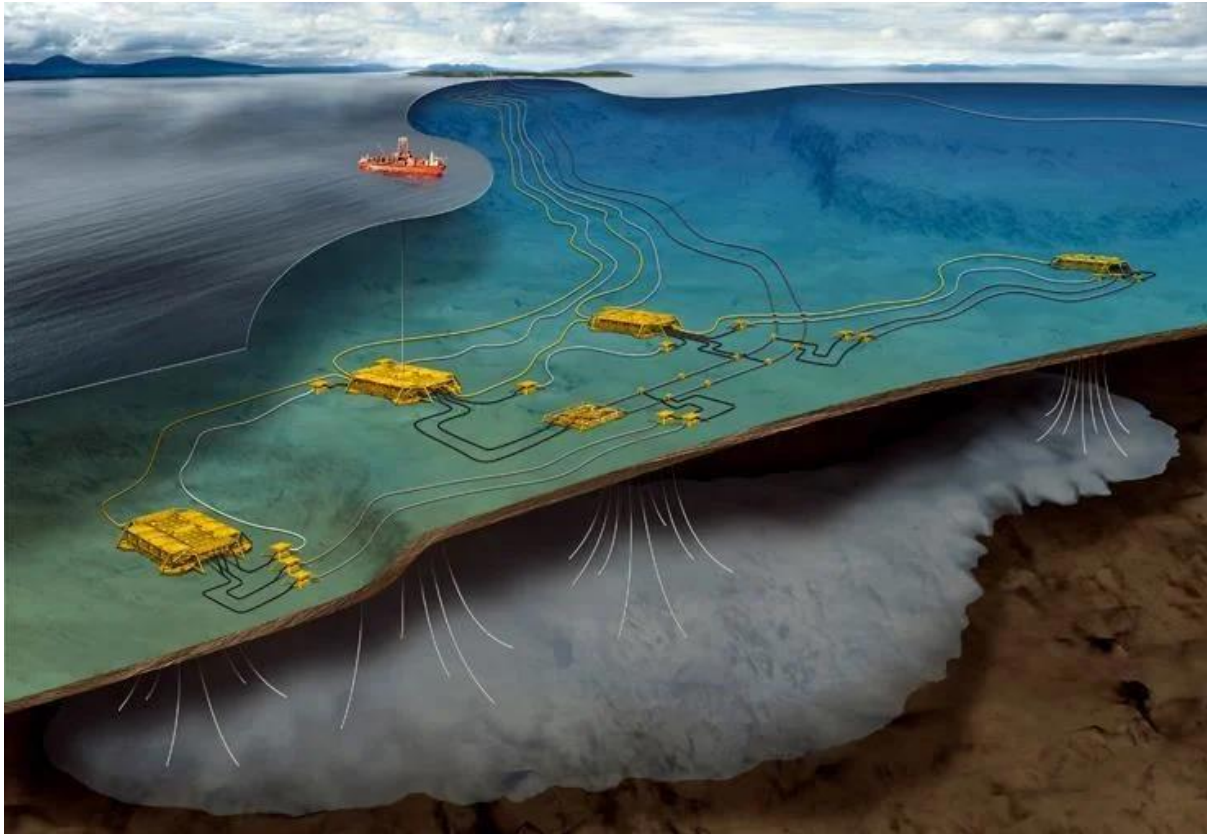


Fig. 1.2. The Ormen Lange gas field in the Norwegian Sea. Adapted from [8]

Oil and gas fields may be developed initially using subsea systems; however, it is an excellent way to further expand and enhance the production of existing fields, especially fields whose production would otherwise decline. Satellite systems consisting of production and injection wells dispersed over a large area can stimulate the reservoir to enhance the production significantly. Also, fields in deeper and more remote waters may prove to be profitable, or even only physically feasible, using a subsea solution – as seen by the rise in subsea well completions in correlation with deep-water field developments [9, 10]. Additionally, the sole use of a subsea solution may be favourable for certain fields, depending on several factors, such as the field layout and existing nearby infrastructure. Offshore oil and gas field developments with wells and associated equipment below the water surface, normally placed on the seabed, are referred to as subsea production systems (SPSs) [9].

An SPS consists of various components, including [9]:

- Drilling systems
- Christmas trees and wellheads
- Umbilicals, risers and flowlines
- Manifolds and jumpers
- Control systems

The produced hydrocarbons flow from the reservoir through the production casing into the Christmas tree, where it is controlled and directed by valves. We distinguish between two types of Christmas trees: Dry trees and wet trees. Dry trees are found onshore, and offshore on topside of fixed platforms, tension-leg platforms, and deep-draft floaters. Dry trees are placed on rigid risers and cannot be used on free-floating facilities. Unlike dry trees, wet trees are placed on the seabed in conjunction with subsea wells, hence the name. A vertical dual-bore wet tree can be seen in Fig. 1.3.

From the wet tree the hydrocarbons go through a jumper to a manifold, where the flow from several wells can be led into a flowline. Depending on the constituents, the hydrocarbons now have to be processed to prepare them for further transport. This can be done either subsea to constitute the SPS or topside. After being processed, the hydrocarbons are transported to refineries onshore by shuttle tankers or pipelines [11].



Fig. 1.3. Subsea Christmas tree. Adapted from [12]

This means that to extract hydrocarbons from offshore reservoirs efficiently and safely, a large amount of equipment and structures must be installed on the seabed.

1.1.3 Future trends

Apart from the oil and gas industry, other evolving sectors require marine lifting operations. The recent emergence and growth of renewable energy sources have highlighted the need for new knowledge and skills related to installation and lifting operations. Offshore wind-power production has increased in recent years, and several projects are on the horizon [13]. Policymakers have stepped up their efforts to support the development of a more sustainable energy economy. The new technologies that will make this happen are expected to lower costs and provide a more efficient and clean energy supply. Wind and solar power are currently the cheapest sources of new electricity generation in most markets. Clean energy technology is expected to become a significant new area of investment and employment [4].

The energy sector is expected to remain under increasing pressure in the coming decades. Over three-quarters of the greenhouse gases that have been released into the atmosphere since the pre-

industrial age have been attributed to the energy sector. The energy sector is the main contributor to climate change and is expected to be at the forefront of addressing the issue. The rapid development and growth of new energy sources are expected to impact the global economy significantly. The increasing number of people and the rising demand for energy services are expected to strain the energy system [4].

Carbon capture and storage (CCS) might grow to be a large-scale industry in the future to reduce the amount of carbon dioxide in the atmosphere. To achieve the so-called two-degree goal suggested by Yale economist William Nordhaus in the 1970s and later adopted by the Intergovernmental Panel on Climate Change (IPCC), we must resolve to CCS [14, 15]. The planned initiatives and policies on nuclear power and electrification are insufficient to reduce the amount of carbon dioxide in the atmosphere to the required level. The CSS technology can capture carbon dioxide from power plants fired on fossil fuels and waste, cement factories and steelworks. The captured carbon dioxide can then be transported and injected into oil reservoirs [15]. *Langskip* is a project funded by the Norwegian government comprising capture, transport, and storage of carbon dioxide [16]. Additionally, subsea shuttle tankers are being conceptualised and are planned to carry out transport of captured carbon dioxide to subsea wells [17].

Marine mineral mining is also an industry that could turn into a considerable sector. Various factors have led to the increasing interest in the exploration and harvesting of seabed minerals. The current investment plans for the mineral supply are insufficient to meet the needs of the electric vehicle, wind turbine, and solar panel industries [18, 19]. Although there are concerns related to seabed mining, such as weakening of the seabed biodiversity and possibly damage to its ecosystem, it may offer a faster road towards electrification of the transport and energy sector. Nature- and wildlife-protection organisations, and several international companies, are sceptical of deep-sea mineral mining for this reason [20].

1.2 Subsea structures and equipment

There exists a vast number of different structures and equipment that are installed on the seabed. Even though sectors such as aquaculture and renewable energies also use such equipment, this thesis will mainly focus on the oil and gas industry. This section will present some of the leading equipment used in this industry. An example of what a typical subsea field may look like can be seen in Fig. 1.4.

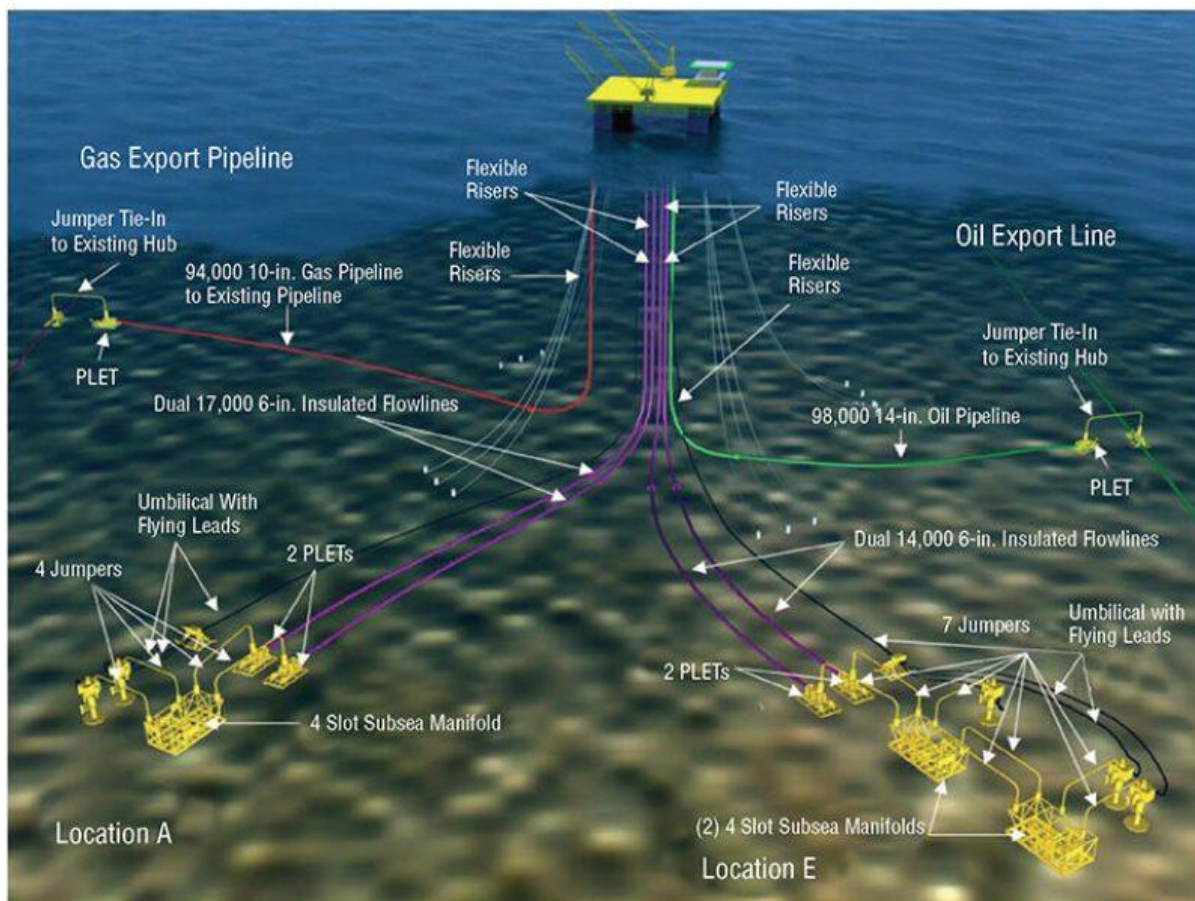


Fig. 1.4. Field layout of the Who Dat field in the Gulf of Mexico. Adapted from [21]

1.2.1 Pipeline end terminations

Pipeline end termination (also called pipeline end modules and pipeline end manifolds) (PLET) is a type of structure used at the end of a pipeline. An inline structure (ILS) is typically located in the middle of a pipeline. These structures connect pipelines together, act as an interface between the pipeline and jumper or riser, hold valves actuated by remotely operated vehicles (ROVs), and accommodate for chemical injection and pigging facilities. The foundation of the modules may be mud mats or a single suction pile [9].

1.2.2 Jumpers

A subsea jumper is a component used to connect equipment such as Christmas trees, PLETs and manifolds, and the risers and flowlines of a well. It can also be used to inject fluids into a well. The offset between the equipment affects the jumper's characteristics and length. The jumper should be designed to be flexible enough to allow for expansion and contraction in response to the changes in pressure and temperature. It should also be rigid enough to withstand the external environmental loads. There are also flexible jumpers, which are more versatile [9].

1.2.3 Subsea wellheads and Christmas trees

The term wellhead refers to a pressure-containing component located at the surface of an oil well. It can be either on the offshore platform, onshore or placed on the seabed (subsea well). Wellheads mark the end point of the well. On top of the wellhead sits the Christmas tree. These components provide an interface for various operations such as drilling, completion and testing. The Christmas trees, which are systems of pipes, valves, fittings, and connections, can be manually operated by divers or ROVs or by hydraulic and/or electrical signals [9].

1.2.4 Manifold

A subsea manifold is an integral part of an oil and gas field's system that allows engineers to simplify the design and operation of the system. It reduces the number of pipelines and risers in the system. A manifold is placed on the seabed to collect the hydrocarbons from producing wells or to inject water or gas. Various manifold applications exist; some act as PLETs and others host extensive processing facilities. They can be anchored to the seabed using piles or skirts. The size of a subsea manifold is influenced by various factors such as the number of wells and the pipeline system's throughput [9].

1.2.5 Integrated template structure

The subsea structure under consideration in this work is based on Nils Olav Hauge's master thesis [22]. It is a subsea integrated template structure (ITS) for oil and gas production. The template is a steel structure that serves as a frame for subsea equipment like Christmas trees, manifolds, pumps, and control units (Fig. 1.5). Its geometry ensures the SPS's integrity and protects it from dropped objects and fishing activity. Hence the template structure is an essential part of many SPSs.



Fig. 1.5. ITS structure for the Maria subsea field in the Norwegian Sea. Adapted from [23]

A problem with such subsea templates is their large added mass, which complicates the splash-zone crossing. The suction anchors contribute significantly to the large added mass. The subsea template in this work has four suction anchors. They are designed to keep the template in place, both horizontally and vertically [24].

In order to safely install components and structures on the seabed, we should investigate their hydrodynamic behaviour and do a thorough risk analysis of the lifting operation. A rough sea state might cause damage to the asset, installation vessel, or other equipment and danger to personnel. Deploying a subsea structure and lowering it through the splash zone is a critical part of its lifetime [25]. A structure may experience loads that can cause irreversible damage and thus delay the installation, which may result in severe economic consequences for the involved parties. Personnel safety is also of utmost importance. The hazards that may arise during the operation has to be identified and accounted for.

1.3 Marine crane-lifting operation

Due to the potentially rough environment and the uncertainty surrounding the marine environment, the installation of a subsea asset such as a template is often carried out with high risks. One of the most challenging activities of implementing an SPS is installing the equipment on the seabed. High costs of the dedicated vessels used for these operations. To minimise these costs, new methods and techniques are being developed [26].

The asset that is being lifted must be transported to the desired location. A designated transportation vessel can be utilised, which is usually the case for heavy constructions. Lighter constructions can be loaded directly onto the crane vessel inshore. According to DNV's recommended practice H103 *Modelling and Analysis of Marine Operations* [27], crane-lifting operations may be divided into two categories related to the weight of the lifted object. A *light lift* is the lifting of a relatively small object – less than 1-2 % of the displacement of the crane vessel. In contrast, a *heavy lift* is the lifting of an object exceeding 1-2 % of the displacement of the crane vessel.

There are four main phases of a subsea lift [27]. These four phases of the lifting operation of an ITS are described in the following sections.

1.3.1 Lift-off and in-air manoeuvring

The crane hook is connected to the lift rigging, which is comprised of slings attached to the lift eyes on the ITS. After the seafastening has been removed completely, the crane lifts the ITS and swings it out overboard.

1.3.2 Splash-zone crossing

The ITS is lowered and eventually hits the water surface. This is called the splash zone, as it usually generates water splashing. The ITS moves from being in the air to be fully submerged in water.

1.3.3 Deeply submerged

As lowering continues, the ITS moves deeper into the water and reaches a state called deeply submerged. This phase is generally between the water surface and the seabed, and the lifted asset can remain in this phase for a relatively long period depending on the water depth. ROVs can monitor the asset while submerged.

1.3.4 Landing

The landing should be meticulously performed to ensure the asset is correctly placed on the seabed. Clump weights can be placed on the seabed prior to the lifting operation. ROVs can then connect tugger lines from the ITS to these clump weights, and the ITS can be carefully winched into place. It is difficult to control an object at the end of the crane wire from the crane vessel. When the ITS is placed where it should be, the suction anchors will start to penetrate the surface. With the help of ROVs, the suction-anchor ventilation holes can be opened or closed. When open, the weight of the ITS will push the suction anchor into the seabed. If closed, the pressure inside the suction anchor will prevent it from further penetrating the seabed. The ITS can be levelled, lowered, or settled by opening and closing specific ventilation holes/hatches and paying out or reeling in the crane winch.

1.4 Objective

This thesis aims to analyse the uncertainties and risks associated with the lifting operation of installing an ITS. Two different models of the ITS are being investigated. The difference between the models is the geometry of their suction anchors, which will be elaborated on later. The models are made in the software OrcaFlex, and time-domain simulations will be run and analysed.

In addition to the numerical analysis, a risk assessment of the lifting operation is performed. The goal is to identify hazards during the operation and find risk-reducing measures to ensure that the activity can be executed safely regarding the risk acceptance criteria.

The marine operation in question is a typical installation operation on the Norwegian continental shelf (NCS).

1.5 Thesis structure

This thesis is divided into seven main chapters. The first part of the thesis focuses on the numerical simulations. In chapter 6, the risk assessment is performed. The final chapter has the conclusions and recommendations for future work.

Chapter 1

In this chapter, the topic of interest is presented. The industry's history is outlined as well as the impact the industry has had in Norway. Moreover, the industry trends for the future are explained.

Chapter 2

In addition to general theory on vessel motion and weather, the theory behind the numerical simulations is presented. An explanation of the hydrodynamic forces is also provided.

Chapter 3

The software and numerical models are covered in this chapter. The calculations for the hydrodynamic models are described.

Chapter 4

This chapter covers the operational criteria for the splash-zone crossing.

Chapter 5

Chapter 5 contains the results from the numerical simulations. The time history of the splash-zone crossing is interpreted, and Gumbel probability papers are generated.

Chapter 6

The risk assessment is conducted in this chapter. Apart explaining the standard practice in the industry, it contains the risk assessment for the four phases of the lifting operation.

Chapter 7

The conclusions of the work and recommendations for future work are given in this chapter.

2 Theory

This chapter explains the theory behind the numerical model and other theories related to marine lifting operations.

2.1 Waves

Although waves are generated differently, waves generated by wind are usually the main concern when it comes to lifting operations. The waves at sea are irregular and random and can be modelled by combining a set of linear waves – called a linear random wave model [28]. Linear waves are modelled considering a set of assumptions.

Regular waves are sinusoidal, and their surface profile is described as a function of horizontal position, x , and time, t (Equation (2.1)).

$$\xi(x, t) = \xi_0 \sin(\omega t - kx) \quad (2.1)$$

where ξ is the surface elevation, ξ_0 is the amplitude, ω is the angular wave frequency and k is a constant.

2.1.1 Irrotational flow

Using the irrotational flow theory, also called potential flow theory, we assume the water to be an incompressible fluid with no shear forces between the fluid particles. This assumption is valid for fluid flow far from the seabed and any constructions (boundaries). Mathematically the irrotationality is represented by the cross product of the gradient, ∇ , and the velocity in all three dimensions, \vec{U} , being a zero vector (Equation (2.2)).

$$\nabla \times \vec{U} = \begin{vmatrix} \vec{i} & \vec{j} & \vec{k} \\ \frac{\partial}{\partial x} & \frac{\partial}{\partial y} & \frac{\partial}{\partial z} \\ u & v & w \end{vmatrix} = \vec{0} \quad (2.2)$$

The compressibility is also zero (Equation (2.3)), which means that the density of the system does not change over time.

$$\nabla \cdot \vec{U} = 0 \quad (2.3)$$

A new function called the potential function is introduced (Equation (2.4)).

$$\varphi = \varphi(x, y, z, t) \quad (2.4)$$

Its partial derivatives with respect to three orthonormal directions x , y and z , are proposed to be equal to the velocities in these directions, u , v and w , respectively. For such a function to exist, Equation (2.5) must be true – hence the flow must be irrotational. By further assuming that the flow is incompressible and using the definition of the velocity potential function, the second-order Laplace differential equation can be derived (Equation (2.6)).

$$\frac{\delta}{\delta x} \left(\frac{\delta \varphi}{\delta x} \right) + \frac{\delta}{\delta y} \left(\frac{\delta \varphi}{\delta y} \right) + \frac{\delta}{\delta z} \left(\frac{\delta \varphi}{\delta z} \right) = 0 \quad (2.5)$$

$$\nabla^2 \varphi = 0 \quad (2.6)$$

To solve the Laplace equation (Equation (3.5)), we use the following boundary conditions:

- Bottom boundary condition
- Wall boundary condition
- Kinematic free-surface boundary condition
- Dynamic free-surface boundary condition

These boundary conditions are based on the physical restrictions of the fluid, such that the fluid cannot flow through the bottom (Equation (2.7)) nor the side walls, e.g., a ship hull. The fluid surface is defined as $z = 0$, and the bottom boundary is located at $z = -d$. Similarly, the fluid cannot flow through the surface. The kinematic free-surface boundary condition (Equation (2.8)) is equal to the time derivative of the surface profile, ξ [29]. Equation (2.9) is derived using assumptions and linearisation of the boundary conditions.

$$\left. \frac{\delta \varphi}{\delta z} \right|_{z=-d} = 0 \quad (2.7)$$

$$\left. \frac{\delta \varphi}{\delta z} \right|_{z=0} = \frac{\delta \xi}{\delta t} \quad (2.8)$$

$$\xi = - \left. \frac{1}{g} \frac{\delta \varphi}{\delta t} \right|_{z=0} \quad (2.9)$$

Equation (2.8) and the time derivative of Equation (2.9) can now be combined to find Equation (2.10), which is valid for $z = 0$.

$$\frac{\delta^2 \varphi}{\delta t^2} + g \frac{\delta \varphi}{\delta z} = 0 \quad (2.10)$$

The Laplace equation can now be solved and the velocity potential, φ , can be found (Equation (2.11)).

$$\varphi(x, z, t) = \frac{\xi_0 g}{\omega} \frac{\cosh k(z + d)}{\cosh kd} \cos(\omega t - kx) \quad (2.11)$$

From the velocity potential, we can derive the velocities. However, the reasoning is based on the incompressibility and irrotational flow assumptions. In addition, the boundary conditions have been linearized, and the wave theory is thus linear [29]. Now the surface profile (Equation (2.12)) can be found.

$$\xi = \xi_0 \frac{\cosh k(z + d)}{\cosh kd} \sin(\omega t - kx) \quad (2.12)$$

On the surface, $z = 0$, we obtain the definition of a regular wave (Equation (2.1)).

2.1.2 Wave spectrum

The wave spectrum gives us a description of the energy of a sea state. The discrete Fourier transform can be found for a measured time series of the surface elevation using the fast Fourier transform, and the spectral density function can be estimated. Several models exist for the wave spectrum, such as Pierson-Moskowitz, Joint North Sea Wave Project (JONSWAP) and Torsethaugen. The models are based on a fully-developed sea, growing wind sea and combined sea, respectively [30, 31]. In this work, the JONSWAP model will be used and is given by Equation (2.13).

$$S_{\xi\xi}(f) = 0.3125 h_s^2 t_p^{-4} f^{-5} \exp\{-1.25 t_p^{-4} f^{-4}\} (1 - 0.287 \ln(\gamma)) \gamma^{\exp\left\{-0.5 \left[\frac{f-f_p}{\sigma f_p}\right]^2\right\}} \quad (2.13)$$

where f is the wave frequency, h_s is the significant wave height, t_p is the peak period, $f_p = 1/t_p$, and

$$\sigma = 0.07 \text{ when } f \leq f_p \text{ and } 0.09 \text{ otherwise.} \quad (2.14)$$

The peak enhancement factor can be found by

$$\gamma = 42.2 \left(\frac{2\pi h_s}{g t_p^2} \right)^{\frac{6}{7}} \quad (2.15)$$

2.2 Vessel motion

A floating vessel has six degrees of freedom (DoFs); three translations and three rotations (Fig. 2.1). The type of marine operation in question dictates which DoFs are the most important. For lifting operations, roll, pitch and heave accelerations are the most critical [32].

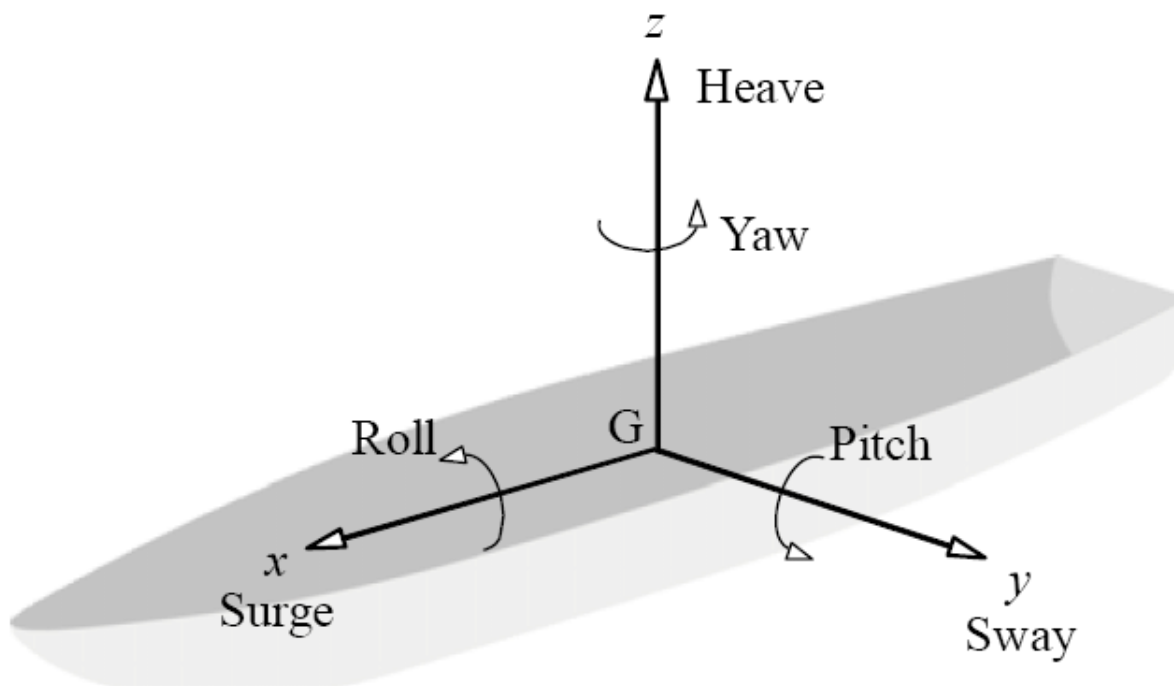


Fig. 2.1. The six degrees of freedom of a vessel. Adapted from [33]

The response amplitude operator (RAO) of a vessel is a description of its motions in the frequency domain. It is the ratio between the response motion and the wave amplitude. The heave RAO is given in Equation (2.16).

$$RAO = \frac{z_0}{\xi_0}(\omega) \quad (2.16)$$

where z_0 is the heave amplitude.

2.2.1 Crane-tip motion

A point of particular interest for marine lifting operations is the crane tip. The translations in the crane tip can be expressed by the following system (Equation (2.17)):

$$\begin{pmatrix} x_p(t) \\ y_p(t) \\ z_p(t) \end{pmatrix} = \begin{pmatrix} x(t) \\ y(t) \\ z(t) \end{pmatrix} + \begin{pmatrix} 0 & -\psi(t) & \theta(t) \\ \psi(t) & 0 & -\phi(t) \\ -\theta(t) & \phi(t) & 0 \end{pmatrix} \begin{pmatrix} x_{0p} \\ y_{0p} \\ z_{0p} \end{pmatrix} \quad (2.17)$$

where x , y , and z are surge, sway and heave, and ϕ , θ and ψ are roll, pitch and yaw, respectively [34]. Op denotes the distance from the vessel's global coordinate system to the local coordinate system in the crane tip.

The vessel's roll motion can induce significant motion in the crane tip. Therefore, to avoid vessel roll motion, the ship can be directed towards the waves – head sea. However, a significant effect that is often taken advantage of in lifting operations is the shielding effect. The sea is calmer in the wake of a stationary vessel, and the structure might be more protected in that zone (Fig. 2.2). Nevertheless, it is a trade-off between reducing induced crane-tip motion by vessel roll and the calmer sea state in the shielded zone [35].

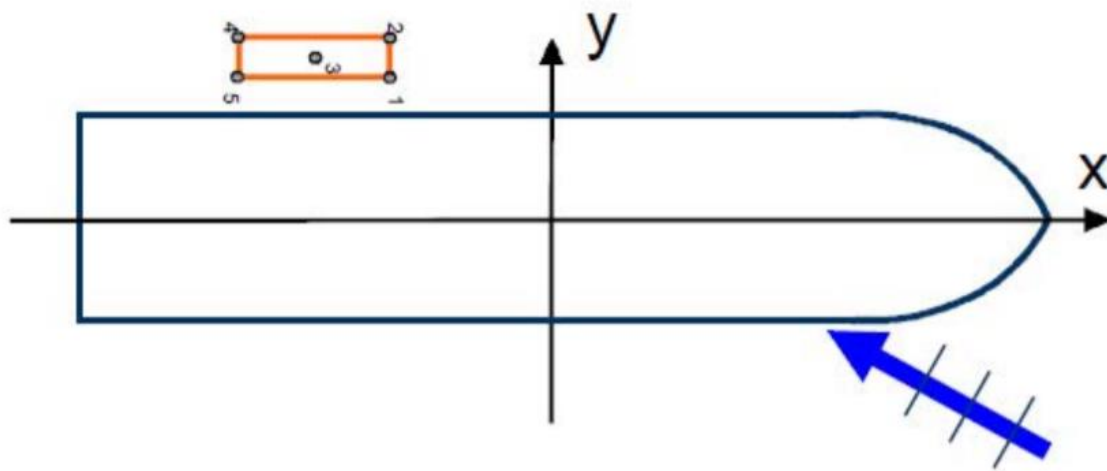


Fig. 2.2. The shielding effect. Adapted from [35]

2.3 Dynamic loads for splash-zone crossing

Three of the most significant loads during the splash-zone crossing are the added mass, slamming and drag force. With the aid of the Morison equation, we can predict the forces on slender structures, i.e., structures with dimensions smaller than the typical wavelengths, usually

$$\lambda = 5D \quad (2.18)$$

where λ is the wavelength and D is the member's diameter or projected cross-sectional dimension [27].

The hydrodynamic forces from the Morison equation (Equation (2.19)) consist of two terms: the first being the inertia forces and the second the drag forces.

$$F(t) = \rho V(1 + C_A)\dot{v} + \frac{1}{2}\rho C_D S v |v| \quad (2.19)$$

where ρ is the fluid density, V is the volume of the structure, C_A is the added-mass coefficient of the structure, \dot{v} is the fluid-particle acceleration, C_D is the drag coefficient of the structure, S is the projected area normal to the force direction and v is the fluid-particle velocity.

To accurately model and analyse a marine operation, the appropriate hydrodynamic coefficients must be found [36].

2.3.1 Added-mass coefficient

The added mass (Equation (2.20)), or hydrodynamic mass, is a factor that is multiplied by the fluid-particle acceleration. The product is the force caused by accelerations of the nearby fluid (Equation (2.21)).

$$m_A = \rho V C_A \quad (2.20)$$

$$F_A = m_A \dot{v} \quad (2.21)$$

where m_A is the added mass and F_A is the force caused by the added mass.

2.3.2 Slamming force

The slamming force (Equation (2.22)) is derived from the principle of momentum conservation.

$$F_S = m_A \dot{v} + \frac{dm_A}{dh} v^2 \quad (2.22)$$

where h is the height above the water surface. The slamming force is an important contributor to the dynamics of the lifted object [37]. In the case of constant velocity, the first term disappears, and the slamming force can be written using the slamming coefficient, C_S (Equation (2.23)).

$$F_S = \frac{1}{2} \rho C_S A_P v^2 \quad (2.23)$$

where A_P is the horizontal projected area. The slamming coefficient is defined by Equation (2.24) [27].

$$C_S = \frac{2}{\rho A_P} \frac{dm_A}{dh} \quad (2.24)$$

2.3.3 Drag coefficient

The drag force, the second term in the Morison equation, depends on the Reynolds number, the Keulegan-Carpenter number, and the surface roughness, among other parameters.

For cylinders, the wake amplification factor, ψ , has to be multiplied with the 3D steady-flow drag coefficient, C_{DS} , to approximate the drag coefficient. The 3D steady-flow drag coefficient is found from the product of the 2D steady-flow drag coefficient and a reduction factor. The procedure is described in [27].

2.4 Weather

There are two main classes of marine operations: weather-restricted and -unrestricted operations. The duration of the operation determines its classification. Operations with a reference period, T_R , less than 96 hours, and a planned operation time, T_{POP} , less than 72 hours, are normally weather restricted. T_R is found from Equation (2.25).

$$T_R = T_{POP} + T_C \quad (2.25)$$

where T_C is the estimated contingency time.

Lifting operations concerning subsea templates and similar structures are usually classified as weather restricted, as the duration is unlike to exceed 72 hours [38].

2.5 Probability

Although it is impossible to precisely predict the outcome of an event with high randomness, such as the surface profile of a sea state and consequently marine operations, we can still use probabilistic models to evaluate it. To appropriately assess the sea state, albeit highly random, we can apply probabilistic models. Extreme-value distributions are commonly used when simulating marine operations and are suitable for modelling extreme values for variables such as design load and response [30, 39].

2.5.1 Gumbel distribution

The Gumbel distribution is such an appropriate extreme-value distribution. The cumulative distribution function (CDF) of the maxima, X , of a set of samples of independent and identically distributed variables is defined as

$$F_X(x) = e^{-e^{-\frac{x-\alpha}{\beta}}} \quad (2.26)$$

where α is the location parameter and β is the scale parameter. We can linearise this equation by taking the natural logarithm twice, and we obtain the following:

$$-\ln [-\ln(F_X(x))] = \frac{x - \alpha}{\beta} \quad (2.27)$$

$$y = \frac{x - \alpha}{\beta} \quad (2.28)$$

By introducing y , we now have a linear equation that will generate a straight line (Equation (2.28)). If we plot this straight line together with the empirical data, we obtain a Gumbel probability paper.

3 Numerical model

The software used in this work is OrcaWave and OrcaFlex issued by Orcina, which are commonly used in the industry.

3.1 OrcaWave

The vessel mesh file was uploaded to the OrcaWave software. The dynamic response and loadings were calculated for wave directions ranging from 0 to 180 degrees with a step of 15 degrees. As the mesh is symmetric over the xz-plane (Fig. 3.1), we obtain the results for wave directions up to 360 degrees. In order to appropriately assess the shielding effect of the vessel, field points are added in the OrcaWave model. The sea-state RAO is calculated in each field point. In the horizontal plane, the field points are 5 meters apart. The three layers are placed at sea level and 4 and 8 meters below sea level. This is to ensure accurate results for the totality of the template during the splash-zone crossing.

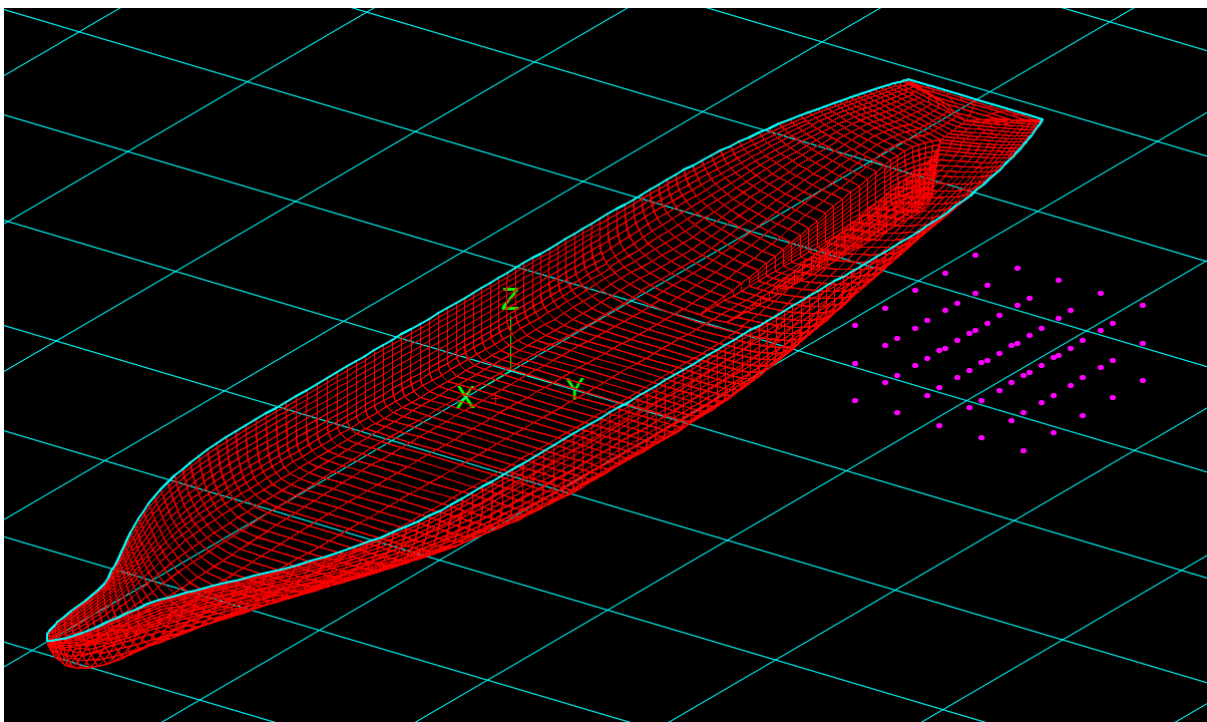


Fig. 3.1. OrcaWave model.

The vessel RAO is presented in Fig. 3.2. The results from OrcaWave are imported into OrcaFlex.

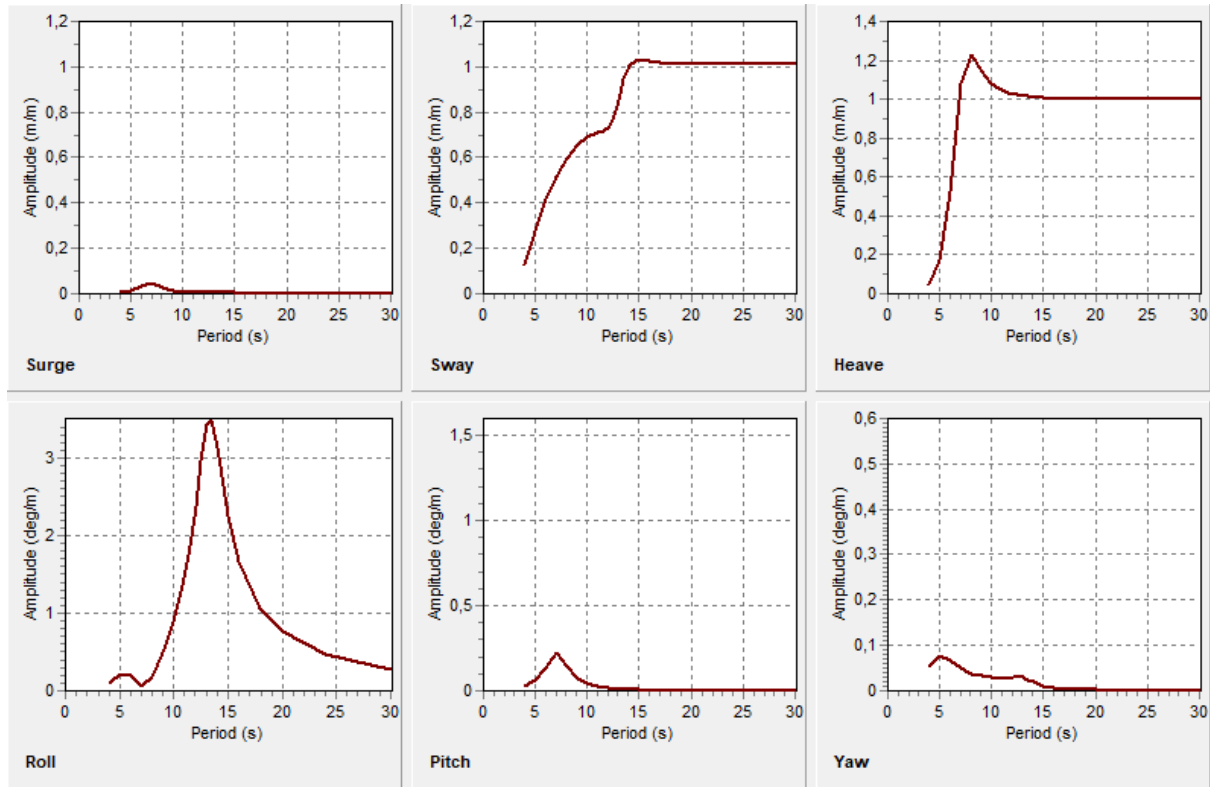


Fig. 3.2. Vessel displacement RAO from OrcaFlex.

3.2 Template models

Two template models are being considered. The difference between the two templates is the suction anchors. The specifications of the templates are given in Table 3.1. The template with the larger-diameter and shorter-height suction anchors is denoted as template A. Template B has narrower and longer suction anchors than template A. The suction anchors on templates A and B are based on [22] and [40], respectively. The mass of the two templates is set to the same value to be able to compare them in the analysis.

Table 3.1. Template specifications.

	Template A	Template B
Outer diameter, OD (m)	6	5.5
Inner diameter, ID (m)	5.96	5.48
Skirt wall thickness, t_s (m)	0.02	0.02
Height, h (m)	7.9	8.225
Top plate thickness, t_t (m)	0.03	0.03
Ventilation-hole diameter, D_v (m)	1	1
Number of ventilation holes, N_v	2	2
Skirt volume, V_s (m ³)	2.97	1.42
Skirt mass, m_s (kg)	23301.17	23301.17
Top-plate volume, V_t (m ³)	0.85	0.71
Top-plate mass, m_t (kg)	6658.61	6658.61
Suction anchor mass, m_{tot} (kg)	29959.78	29959.78
Suction anchor mass, m_{tot} (tonnes)	29.96	29.96
Template mass, m_{temp} (tonnes)	335.00	335.00

3.3 Hydrodynamic forces

The coefficients for the hydrodynamic forces are calculated and put into the numerical models. The methods used for finding the coefficients are described in [27]. Complete calculations can be found in Appendix A.

3.3.1 Added mass

3.3.1.1 Normal-direction added mass for cylinders

From Table A-2 in [27] (Fig. 3.3), we find the ratio between the height and diameter of the suction anchor and interpolate it to find the added-mass coefficient.

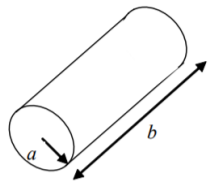
Body shape		Direction of motion	C_A		V_R
			$b/2a$	C_A	
Right circular cylinder		Vertical	1.2	0.62	$\pi a^2 b$
			2.5	0.78	
			5.0	0.90	
			9.0	0.96	
			∞	1.00	

Fig. 3.3. Analytical added-mass coefficient. Adapted from [27].

3.3.1.2 Axial added mass for cylinders

In the same table (Table A-2), we find the added-mass coefficient for a circular disc. However, the trapped water inside the suction anchor also contributes to the added mass and must be included. To accurately model this, the added-mass coefficient is not included in the 6D buoy representing the suction anchor. Instead, three line elements representing the three components of the added mass (Fig. 3.4) have been added to the models.

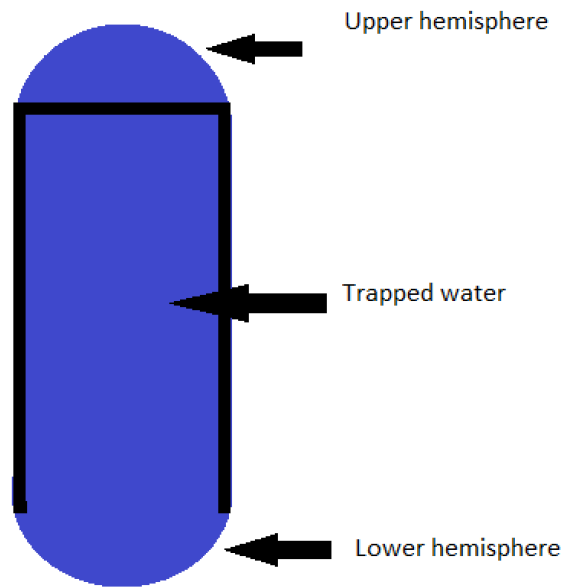


Fig. 3.4. Components of the axial added mass for the suction anchors.

This ensures that the hydrodynamic effects are modelled at the correct depth. The suction anchor and the line elements can be seen in Fig. 3.5.

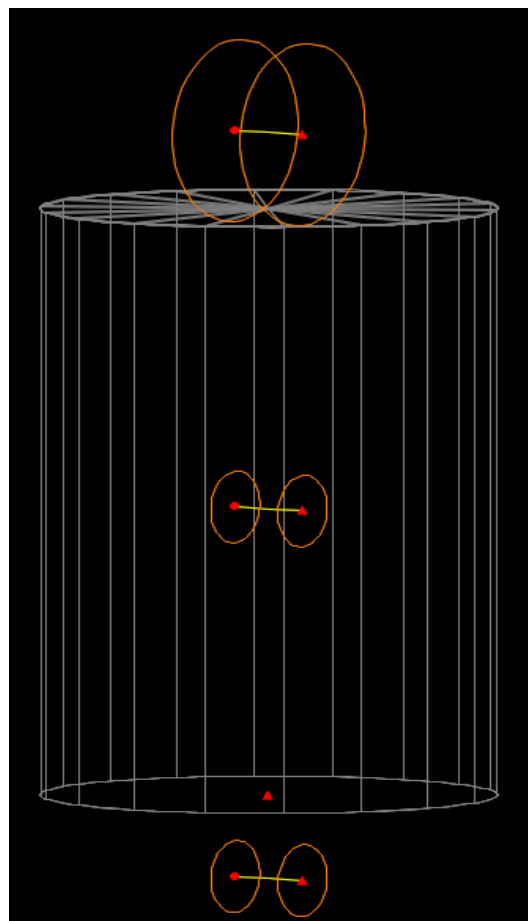


Fig. 3.5. OrcaFlex suction-anchor model with line elements representing added mass.

The line elements are placed in the centre of mass of the volume they represent. In OrcaFlex the added mass can be modelled as a constant value or as variable data. Again, variable data as a function of depth was used to ensure high accuracy. The variable data is based on Figure 3-5 in [27] (Fig. 3.6). It shows the vertical added-mass coefficient, and its derivative of a cylinder normal to the water surface plotted against normalised submergence.

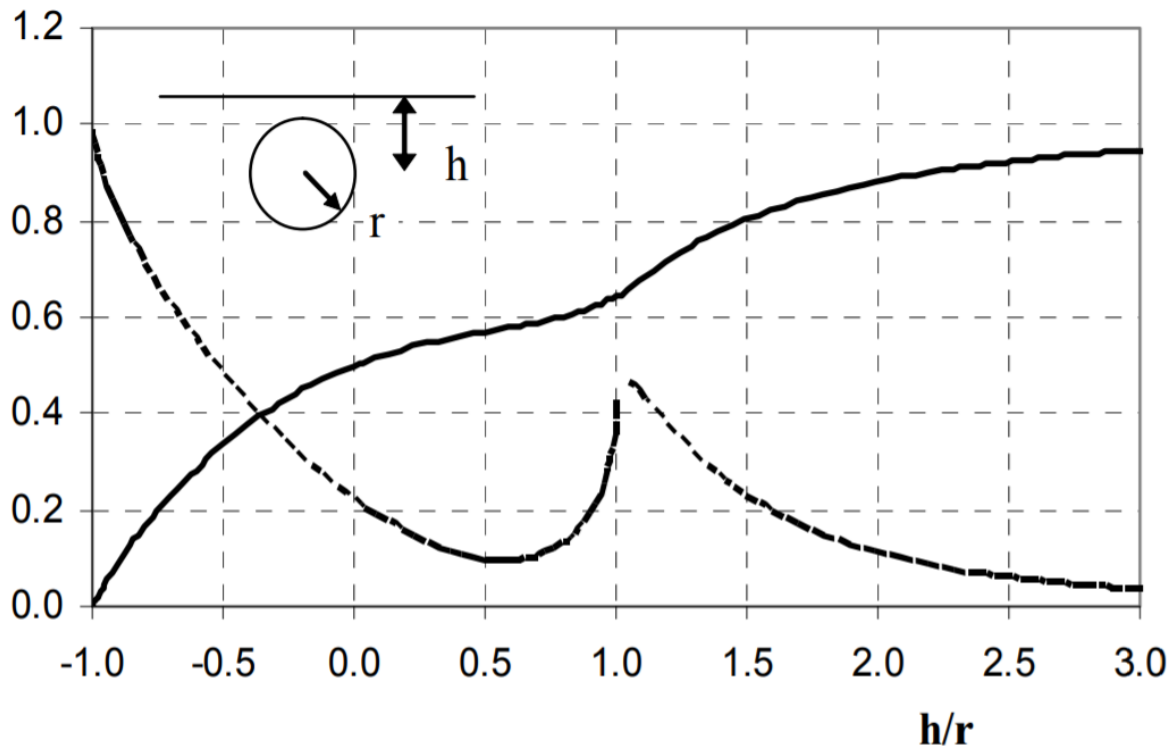


Fig. 3.6. Vertical added-mass coefficient and its derivative of a cylinder of radius r . Adapted from [27]

We introduce the normalised submergence, defined as the ratio between the distance from the water surface and the radius of the submerged object (Fig. 3.7).

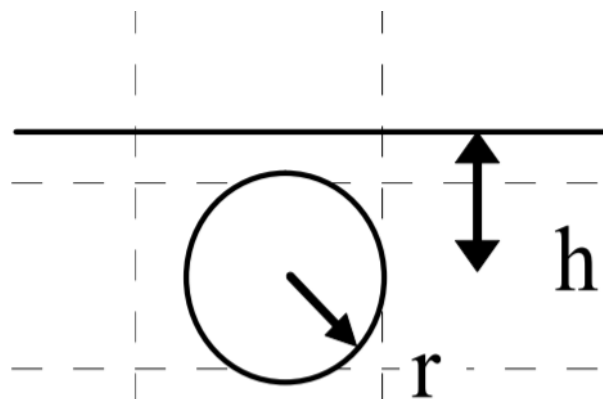


Fig. 3.7. Normalised submergence. Adapted from [27]

The added-mass line elements are defined such that their added mass is activated when the top plate of the suction anchor is submerged, i.e., the distance from the top plate is accounted for in their normalised submergence.

Based on Figure 3-5 in [27] (Fig. 3.6), 20 data points have been generated for the added-mass coefficient and its derivative (rate of change of the added-mass coefficient with respect to normalised submergence, h/r) and presented in Table 3.2.

Table 3.2. Data points generated from Figure 3-5 in [27].

Normalised submergence, h/r	Added-mass coefficient, C_a	Rate of change of added-mass coefficient, dC_a
-1	0.00	0
-0.99	0.01	1
-0.75	0.18	0.7
-0.5	0.35	0.5
-0.25	0.43	0.35
0	0.50	0.22
0.25	0.53	0.15
0.5	0.55	0.1
0.75	0.60	0.13
1	0.65	0.45
1.25	0.73	0.35
1.5	0.80	0.23
1.75	0.85	0.17
2	0.90	0.12
2.25	0.92	0.09
2.5	0.93	0.06
2.75	0.94	0.04
3	0.95	0.03
4	0.96	0.01
5	0.96	0

The normalised submergence for the upper line element (representing the upper hemisphere of added mass) does not have to be altered as its radius equals the distance from the top plate to the upper-hemisphere centroid. Hence the upper line element and the suction anchor top plate will hit the water surface simultaneously. The normalised submergence for the two other line elements, trapped water and the lower hemisphere, must be altered.

The variable added-mass coefficients for the line elements, C_{Ai} , are found by multiplying the added mass, A_{33} , with the added-mass coefficient from Table 3.2, C_a , and dividing by the displaced water, Δ , ((Equation (3.1)). i take the following values: u , t and l standing for *upper hemisphere*, *trapped water* and *lower hemisphere* respectively. The added mass for the top plate (circular disc) is distributed among the upper and the lower line element, so it has to be divided by two.

$$C_{Ai} = \frac{A_{33i}}{\Delta_i} C_A \quad (3.1)$$

3.3.2 Slamming

To model the slamming force, we use the rate of change of the added-mass coefficient. Similar to the added-mass coefficients for the line elements, their slamming coefficients, dC_{Ai} , are found by using the following expression ((Equation (3.2))):

$$dC_{Ai} = \frac{A_{33i}}{\Delta_i} dC_A \quad (3.2)$$

where dC_A is the rate of change of added-mass coefficient from Table 3.2.

3.3.3 Drag

The Keulegan-Carpenter number, KC , is defined as ((Equation (3.3))):

$$KC = \frac{\pi H_s}{D} \quad (3.3)$$

where H_s is the significant wave height and D the diameter of the cylinder [29]. The skirts of suction anchors are usually rusty [24]. Therefore, the surface is assumed to be rough. The method used is described in section 2.3.3.

3.4 Environmental data

The environmental data is presented in Table 3.3. The significant wave height in this work is set to 2 m. The wave direction is set to 165 degrees, and we can take advantage of the shielding effect (Fig. 3.8).

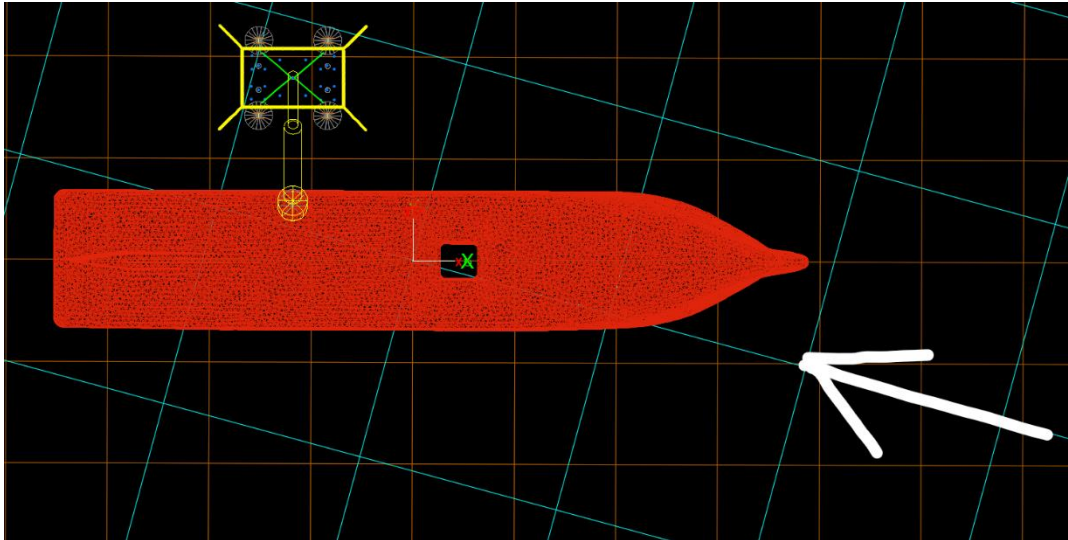


Fig. 3.8. Wave direction.

In time-domain analysis, OrcaFlex uses different wave-component frequencies for the different directions to ensure no correlation [41]. The number of wave directions is set to 20. An appropriate value for the spreading function is 2 for the wind sea [28].

Table 3.3. Environmental data.

Wave-spectrum model	JONSWAP
Significant wave height, H_s (m)	2
Wave direction (deg)	165
Number of wave directions	20
Spreading function, n	2

Four different mean zero up-crossing periods, T_z , are chosen and tested: 4, 6, 8 and 10 seconds. There is thus a total of 200 simulations.

3.5 Crane and lifting wire

The crane in the model has no mass and will therefore not influence the simulation. The position of the crane tip in the global coordinate system is shown in Table 3.4. The global coordinate system has its origin in the centre of gravity of the vessel.

Table 3.4. Coordinates of crane tip.

Coordinate	Value (m)
x	-23.5
y	35.0
z	34.2

The stiffness of the lifting wire is 1238 MN, and its initial length is 8 m.

3.6 Duration and stages

The simulation is divided into several stages. The start time of the simulation is -65 s. The winch starts lowering the template at 0 s and continues the lowering till the end of the simulation at 148 s. The reason for starting the simulation at -65 s is to let the sea state develop before the operation starts. The winch starts at -8 s and reaches the constant pay-out rate of 0.2 m/s at 0 s.

Table 3.5. Simulation stages.

Stage	Start time (s)	End time (s)	Action
Stage 1	-65	-8	Sea state builds up
Stage 2	-8	0	Winch starts
Stage 3	0	148	Winch pays out at constant rate

4 Operational criteria

The dynamic hook load is the limiting factor in this type of operation. The load must not exceed the capabilities of the crane, the wire, and the hook itself. The slings must also be able to handle the loads, and they are normally designed and chosen according to the results from the time-domain simulations [22]. The crane's capacity is 420 tonnes and is the limiting factor in this case. The value is chosen based on the information given in [22] and is listed in Table 4.1.

Table 4.1. Upper load limit for the lifting-wire tension.

Maximum mass (tonnes)	Maximum load (kN)
420	4120.2

According to [27], snap forces shall be avoided, i.e., the hydrodynamic forces acting upwards shall not be greater than the weight of the lifted object. A 10% safety margin is added to this condition (Equation (4.1)). The weight of the template is reduced in water and is found to be 3242 kN.

$$F_{hydrodynamic} \leq 0.9F_{static} \quad (4.1)$$

Table 4.2. Lower load limit for the lifting-wire tension.

Minimum mass (tonnes)	Minimum load (kN)
2.97	29.2

5 Results and discussion

The data collected from the OrcaFlex simulations are used to analyse the time history of the lifting-wire tension. They are then imported into the computer software MATLAB. The MATLAB script can be found in Appendix B. The first stage of the simulation is not included because it is not of interest as it is simply to allow the sea state to build up.

5.1 Time history of tension

The tension of the lifting wire is plotted over time in this section. In Fig. 5.1, the time histories of two different realisations are plotted for template A. The lowering of the object starts in point A. Here, the load equals the template's weight in air. The motion of the vessel determines the motion of the ITS. There are minor vibrations. The ITS penetrates the water surface at point B. At this point, the load gradually decreases. At point C, the suction-anchor top plates hit the water surface. Extreme variations in tension are observed due to the hydrodynamic forces. This is confirmed by the time-series data of the suction-anchor top plate's vertical position (not shown here). The hydrodynamic forces of the template start to decay at point D. Minor oscillations in the structure's submerged weight are observed at the end of the simulation (point E).

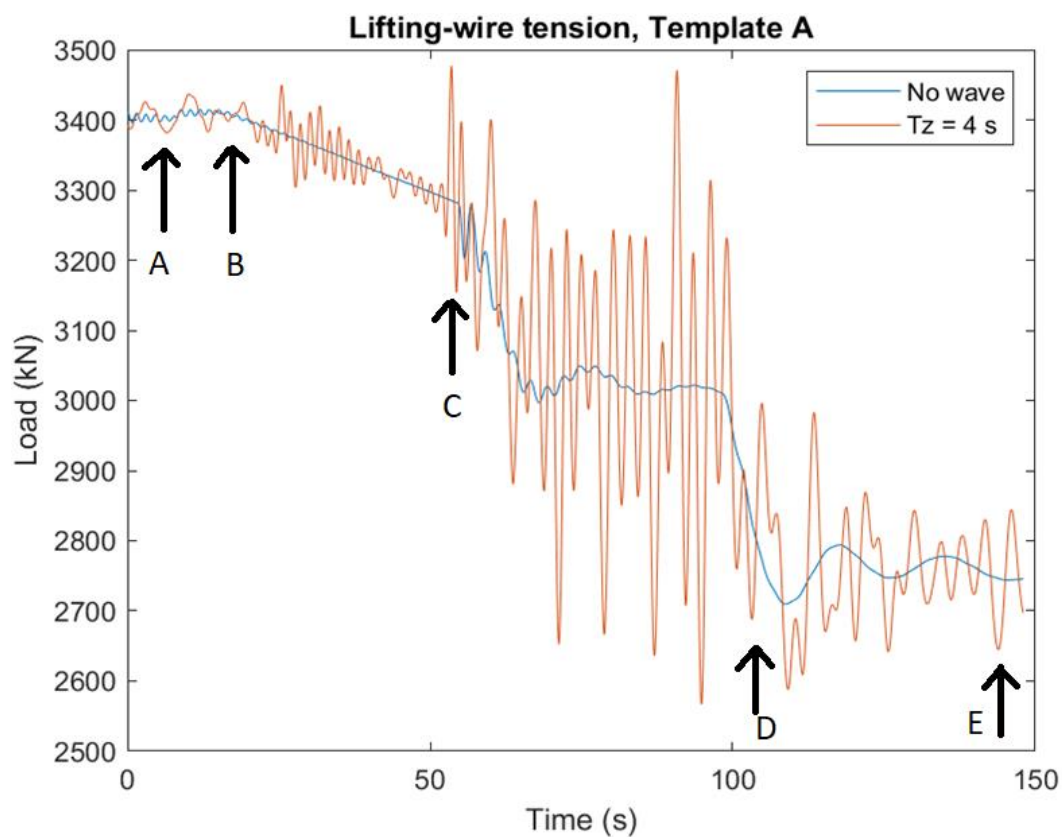


Fig. 5.1. Lifting-wire tension for template A for still water and for $T_z = 4$ s.

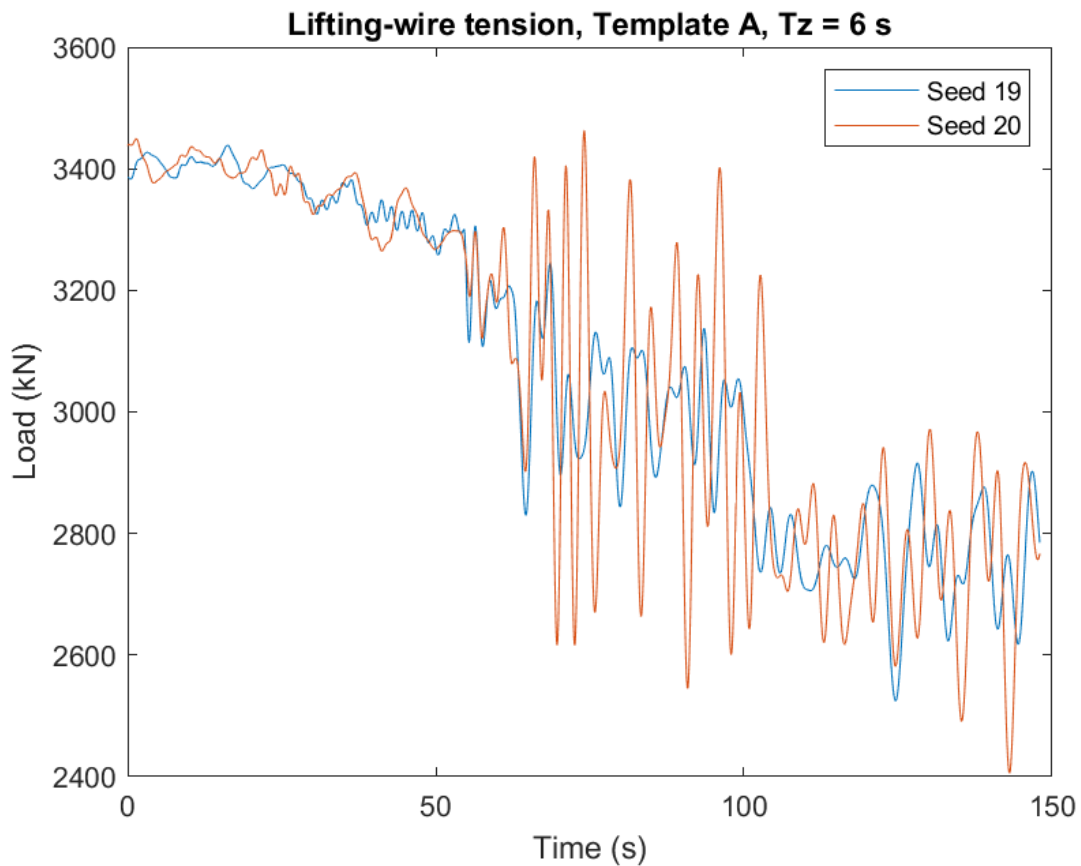


Fig. 5.2. Lifting-wire tension for template A for $T_z = 6$ s for two different seeds.

Despite the parameters being identical, the simulation results can vary greatly for different seeds. OrcaFlex will generate random phases for the wave components using an algorithm. This algorithm is based on the seed and produces a repeatable sequence. Hence the wavetrain for a given seed will always be identical – given that all other sea-state parameters are identical. Therefore, it is possible to repeat an exact wave elevation by using the same seed [41]. In Fig. 5.2, the same parameters for two different seeds are shown.

In Fig. 5.3, the lifting-wire tensions for both templates are shown using the same seed. As expected, the initial parts of the graphs are identical, while the template is hanging in air. When the templates are submerged, the difference in tension becomes apparent. It is under the surface that the hydrodynamic forces in the models are activated. The template with the wider suction anchors, template A, generates higher lifting-wire tension. These findings are coherent with [40]. A reason for the higher tension could be that template A has a higher added mass than template B.

Furthermore, the seed in Fig. 5.3 is the seed that gave the highest lifting-wire tension. The lifting-wire tension exceeds the upper load limit, contrary to all the other seeds. The lifting-wire tension was substantially lower in other realisations. A rocking motion can be seen in the simulation replay.

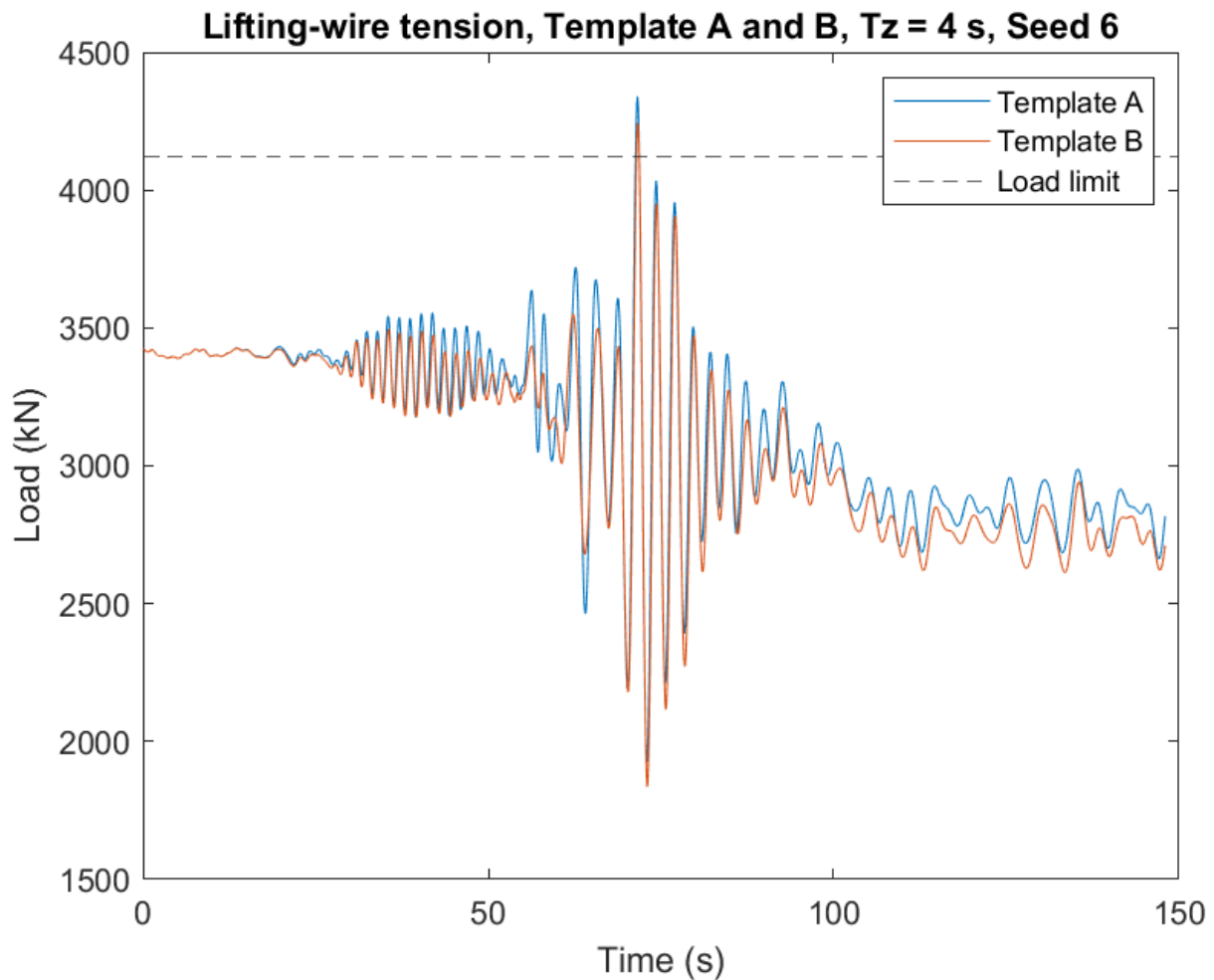


Fig. 5.3. Lifting-wire tension for template A and B for $T_z = 4$ s for same seed.

5.2 Gumbel probability paper

In this section, the Gumbel probability papers for the four different T_z are presented. The lifting-wire tension is placed on the horizontal axis, whereas the vertical axis contains the y introduced in Equation (2.28). The y is labelled Y Gumbel in the Gumbel probability papers. Taking the left-hand side of Equation (2.27) and replacing the CDF ($F_X(x)$) with 0.95, the 95 % threshold can be found (Equation (5.1)).

$$-\ln [-\ln(0.95)] = 2.97 \tag{ 5.1 }$$

The plots reveal that only one of the maxima from the 25 seeds lies above the 2.97 threshold. Hence only one of the maxima belongs to the top 5 % of the Gumbel distribution.

The templates generate quite different Gumbel-fit lines for $T_z = 4$ s with respect to the 95 % line (Fig. 5.4). The template A Gumbel-fit line is located below where the 95 % line and the load-limit line intersect, meaning that it would not meet the criteria of non-exceedance. A very interesting plot feature is the highest value for each template. They appear to be separated from the other values – which is especially the case for the value for template B. These values have been obtained by

chance. The seed that generated these values has produced a sea state that resulted in an especially high dynamic response. The amount of data is therefore of utmost importance. The larger the set of samples, the more accurate the estimates [42]. However, the data seems to follow the Gumbel distribution apart from these two maxima.

A reason for why these two values differ from the rest could be linked to resonance. The generated wavetrain may have caused a vertical oscillation in the region of the natural frequency of the lifting wire. The rocking motion observed in the simulation replay suggests that the resonance originated from the rotation of the template.

All the other values in the Gumbel-fit lines lie below the load-limit line, which can be seen in Fig. 5.5 – 5.7. These T_z are consequently less inclined to induce loads that exceed the load limit – at least in this numerical setup. Another feature of the Gumbel probability papers (Fig. 5.4 – 5.7) worth noting is that the Gumbel-fit line for template A is shifted upwards relative to the Gumbel-fit line for template B with increasing T_z . A possible explanation for this could be that template A's comparatively higher added mass causes it to sink slower. For increasing T_z , the vessel will tend to follow the surface elevation and might not cause such a large vertical motion in the template.

In addition, the lifting-wire tension decreases for increasing T_z , which clearly indicates that the probability of exceeding the load limit is lower for larger T_z .

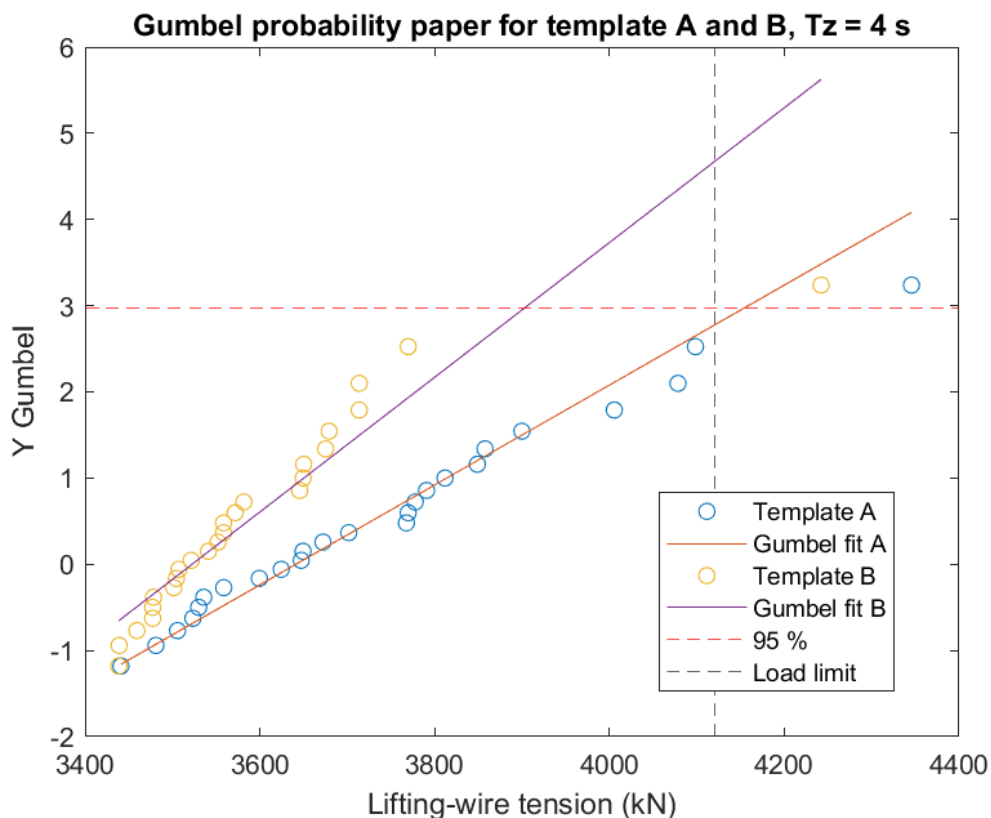


Fig. 5.4. Gumbel probability paper for template A and B for $T_z = 4$ s.

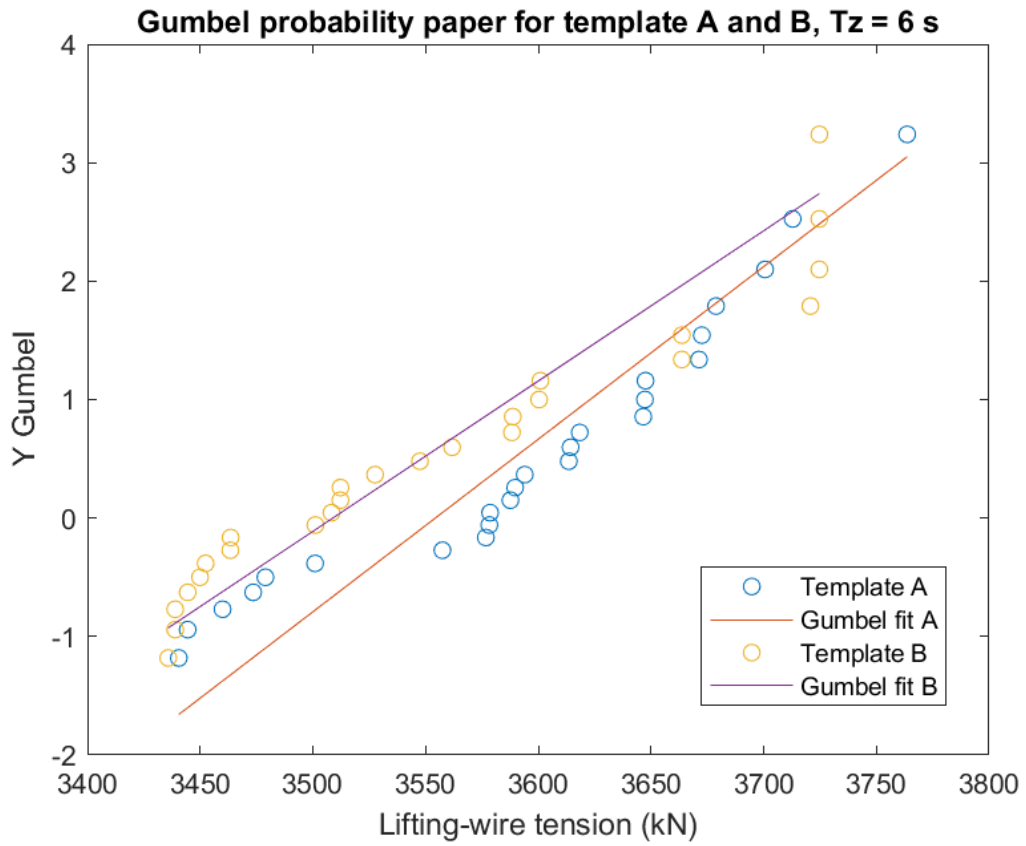


Fig. 5.5. Gumbel probability paper for template A and B for $T_z = 6$ s.

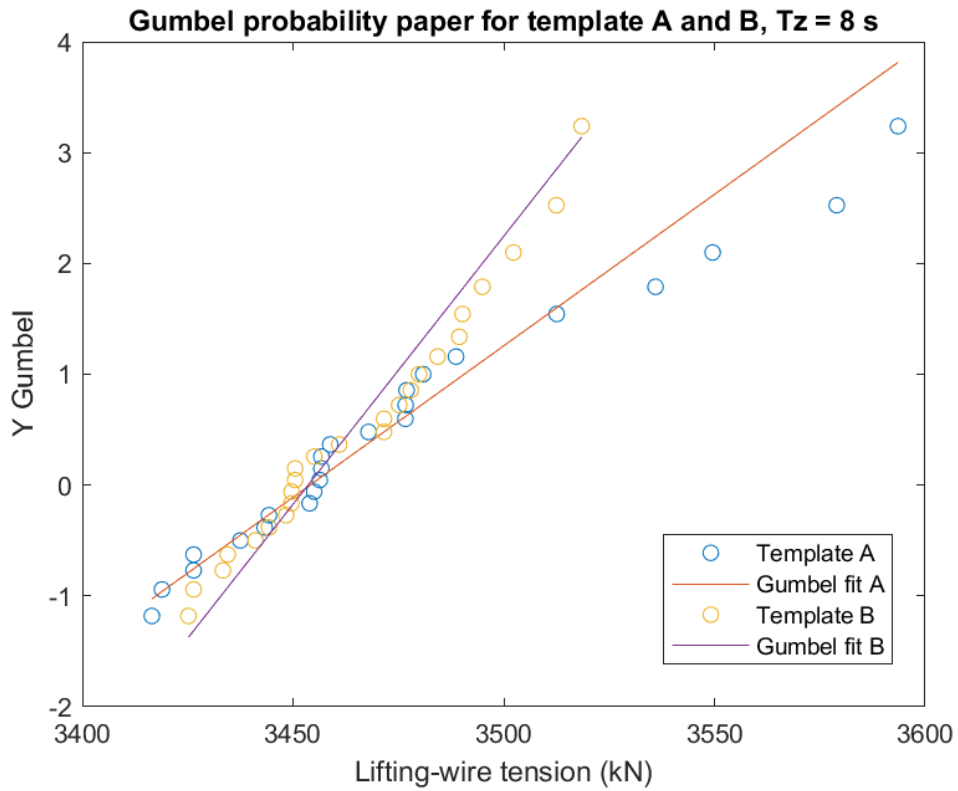


Fig. 5.6. Gumbel probability paper for template A and B for $T_z = 8$ s.

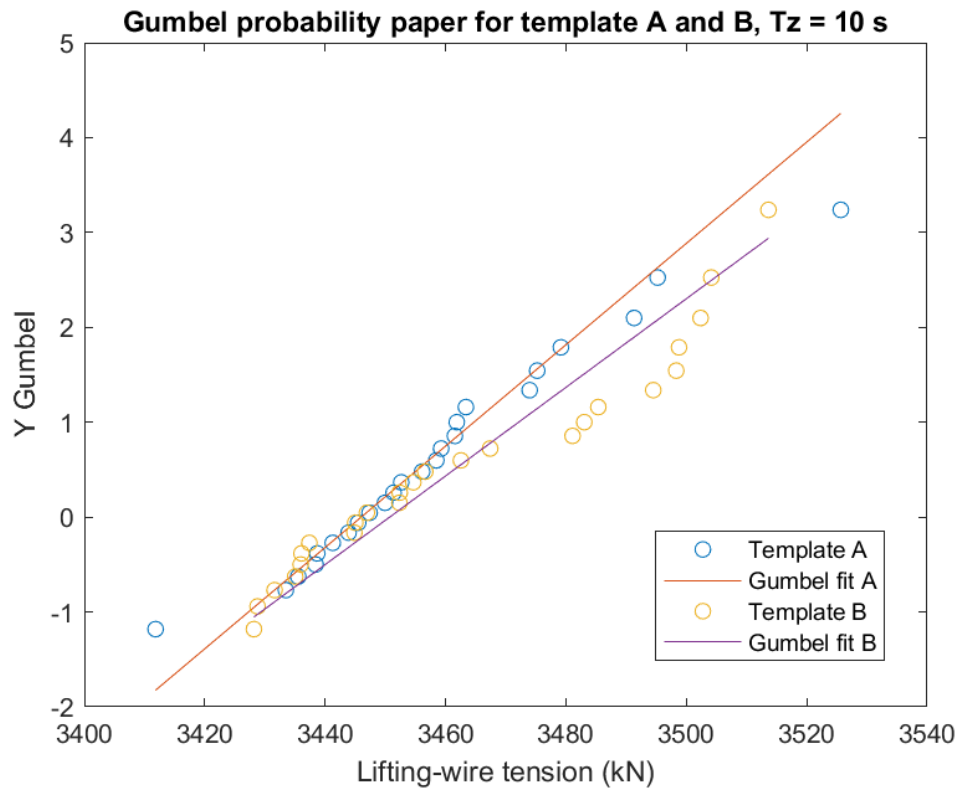


Fig. 5.7. Gumbel probability paper for template A and B for $T_z = 10$ s.

Interestingly, none of the simulations generated values close to the lower load limit of 29.2 kN.

6 Risk assessment

There is no single definition of risk, and it is not always easy to understand. In the literature, various definitions of risk are presented. Some of these include probabilities, chance, and expected values, while others are focused on uncertainties and undesirable events. Some consider risk subjective and epistemic, depending on the available knowledge [43]. Nevertheless, there are clear guidelines on marine operations, such as DNV's recommended practice H101 *Risk Management in Marine – and Subsea Operations* [44] and NORSOK Z-013:2010 *Risk and emergency preparedness assessment* [45].

The importance of assessing the risk of a marine operation has been manifested through the losses and damages in history. The cause of an accident ranges from a change in weather to design errors, including failure in equipment and structures. Furthermore, human errors, misjudgements, and misunderstandings also trigger accidents [46]. The data collected from the various marine operations linked to the installation and operation stages show that 13% of accidents occurred during these stages [47].

A risk assessment aims to create a systematic method to ensure that risk has been appropriately addressed. Hazards (potential threats) must be identified and should be either reduced to an acceptable level or eliminated [48].

In this chapter, I will assess the risk for the lifting operation required to install the ITS described earlier in this work (section 3.2). Such an assessment is usually performed by an analysis team consisting typically of the crane operator, deck foreman, technical safety engineer, safety representative, asset manager, offshore manager, and risk manager. However, in this work, I will perform this task by myself with the help of the resources available and through contact with professionals in the industry. Additionally, the governing principles and common practice in the industry is discussed.

6.1 Risk acceptance criteria

In the Norwegian petroleum industry, the operators are responsible for controlling the health, safety and environment (HSE) issues faced by the company. The companies must perform internal audits to record and objectively evaluate if it fulfils given criteria [49]. In the context of risk assessment, such a criterion is called a risk acceptance criterion. The risk acceptance criterion is normally defined before the risk analyses are conducted. However, Aven and Vinnem [49] has argued that that a predefined criterion might give the wrong focus and also attribute a mechanical character to the criteria. When the risk acceptance criterion in question has been reached, there is no further encouragement to reduce risk. This may pose a threat in the case of modification to the project. A modification could change the risk picture and put the project on hold if the risk acceptance criterion is exceeded due to the modification.

Additionally, Abrahamsen and Aven [50] has criticised the fact that the industry is to define the risk acceptance criteria. They argued that the operators do not necessarily serve the best interests of society. Instead, the authorities, Petroleum Safety Authority Norway (PSA), should play a more active role in setting the limits for risk, like in other countries such as the UK [50].

Although the aforementioned risk experts suggest pre-determined risk acceptance criteria should be used with caution, the common practice in the industry appears to be just that – especially on the NCS [49].

Examples of risk acceptance criteria in the industry could be [49]:

- For the personnel involved in the assessment, the fatal accident rate (FAR) value should be less than 10, where FAR is a measure of number of fatalities per 100 million hours (roughly 1000 employees working lifetimes).
- The likelihood of a person being killed in an accident for one year should not exceed 0.1%.

6.2 ALARP

An important principle in risk analysis is to reduce the risk as low as reasonably practicable (ALARP). The principle of ALARP means that the measure in question should be implemented unless the cost is grossly disproportionate to the benefit [51]. In some instances, a cost-benefit analysis is required to determine the financial implications of a risk-reducing measure. This type of analysis is usually performed when the costs are high. However, low-cost measures such as reorganising work routines can be implemented without thorough analyses.

Applying the ALARP principle usually involves the employment of three risk categories [52]:

1. Negligible risk: The risk is too low to be considered
2. Intermediate risk: Risk-reducing measures should be implemented according to the ALARP principle
3. Intolerable risk: The risk is too high even with appropriate measures in place

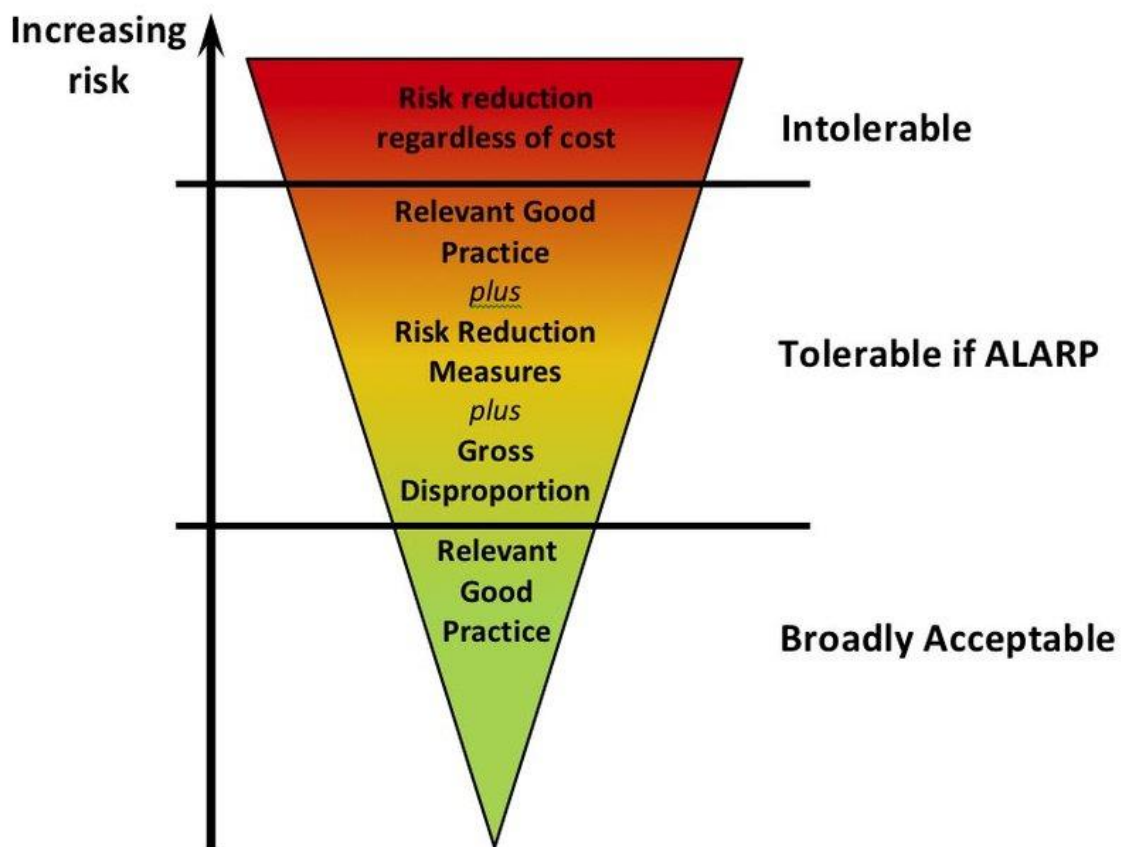


Fig. 6.1. The ALARP principle. Adapted from [53]

The authority involvement in evaluating risk results is more active when the ALARP approach is used. This approach is more comprehensive than simply inspecting the results of a risk assessment – which, simplistically speaking, could be to compare the numerical result from the risk assessment to

the risk acceptance criteria. In order to evaluate the effectiveness of the measure, authorities will need to conduct an extensive evaluation. This process will involve looking for alternatives to the risk-reduction measures identified in the analysis [49].

6.3 The risk assessment process

In Fig. 6.2, the risk assessment process is shown, which is similar to the process diagram in [45]. The first step is to define the objective and scope of the assessment, which in this case is to assess the risk for the installation of an ITS on the NCS. After having defined risk criteria, we have to identify the hazards. From there, we analyse and evaluate the risk. If the risk is found to exceed the risk acceptance criteria, we have to introduce risk-reducing measures. In a professional setting, risk management teams review and monitor the process.

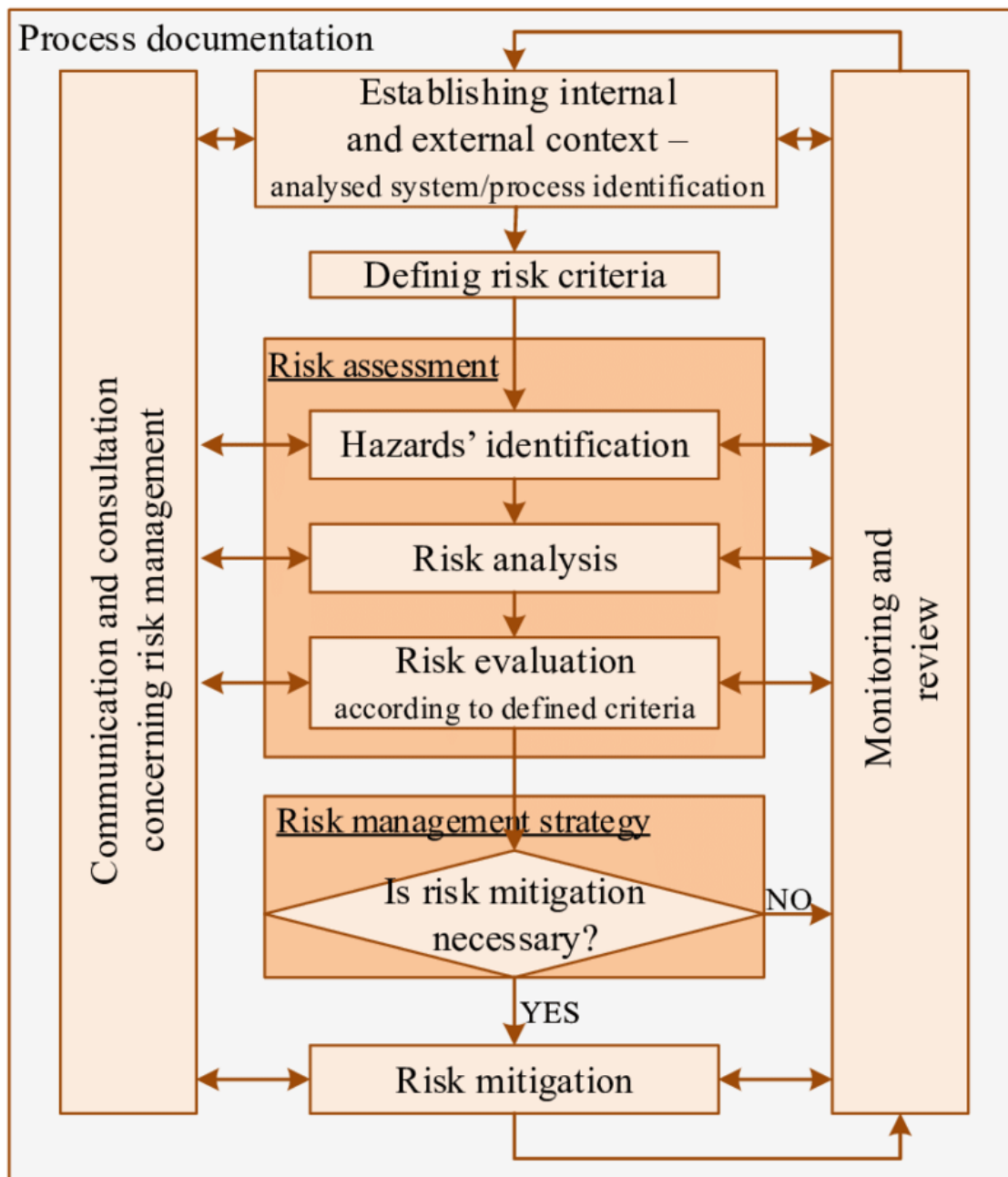


Fig. 6.2. Risk assessment process. Adopted from [54]

Risk can be assessed both qualitatively and quantitatively. Due to the increasing number of scientific and technological applications, there is a continuous discussion about how to measure and describe risk. Most analysts would agree that there is a need for both quantitative and qualitative methods when it comes to assessing risk. For instance, in certain situations, the degree of uncertainties can also be considered a factor that should be considered. In most cases, using knowledge-based probabilities is not ideal because it is hard to justify the support for the numbers [43, 55]. It is, however, a practical and commonly used method in the industry.

In order to display the risk acceptance criteria in this thesis, I have used a risk matrix (Table 6.1). The impact and probability of a hazard determine its value. It is important to underline that the risk matrix is not a risk-analysis method but merely a way to present risk [56]. The hazard value is then assessed compared to limits set in relation to the ALARP principle. The limits in this work are stated in Table 6.2, which are also apparent from the colours in the risk matrix.

Table 6.1. Risk matrix.

Impact category	Risk rating				
	20	50	75	150	300
E (Very high)	20	50	75	150	300
D (High)	10	25	50	75	150
C (Moderate)	5	10	25	50	75
B (Slight)	2	5	10	25	50
A (Negligible)	1	2	5	10	25
Likelihood	1 (Very unlikely)	2 (Unlikely)	3 (Possible)	4 (Likely)	5 (Very likely)

Table 6.2. Risk limits.

Value	Risk
Less than 25	Negligible
25 – 50	Intermediate
More than 50	Intolerable

Four aspects of the hazard impacts have been considered: Health and safety, environment, company reputation and financial cost (

Table 6.3). A common mistake is to use vague terms for the description. Instead of stating that, e.g., the environment will be immensely polluted, exact numbers should be used. The same goes for the probabilities [56].

Table 6.3. Impact description.

Impact category	Health and safety	Environment	Company reputation	Financial cost
E (Very high)	Loss of life, permanent disability, and/or terminal illness.	Severe harm to environment that requires corrective measures. Pollution above 100 000 litres.	Severe and possibly irreversible impact on relationship with authorities, costumers, and general public. Corrective measures required.	More than 10 000 000 NOK.
D (High)	Serious injury or illness that results in dramatically lowered life quality.	Serious harm to environment that requires corrective measures. Pollution up to 100 000 litres.	Serious impact that requires corrective measures. May affect relationship with authorities, costumers, and general public.	Up to 10 000 000 NOK.
C (Moderate)	Injury that results in long recovery time.	Moderate harm to environment that requires corrective measures. Pollution up to 100 litres.	Moderate impact that may require corrective measures.	Up to 5 000 000 NOK.
B (Slight)	Minor injury treatable with first aid. Short recovery time.	Slight harm to environment that requires corrective measures. Pollution up to 10 litres.	Slight impact.	Up to 1 000 000 NOK.
A (Negligible)	Negligible injury. No recovery time needed.	Little to no harm to the environment. Pollution less than 1 litre.	No impact.	Less than 100 000 NOK.

To analyse the risk, I have applied a hazard and operability (HAZOP) study, commonly used in the Norwegian petroleum industry [51]. Additionally, it is suitable for assessing operating sequences and procedures [57]. The study has been performed in accordance with [57]. In addition to the HAZOP approach, which is mainly a qualitative method, I have added a quantitative component to the assessment in the form of a risk rating. Each hazard is given a risk rating based on the risk matrix (Table 6.1). The hazards also have a risk-reducing measure (*actions required* in the HAZOP studies in **Error! Reference source not found.** – 6.7). The HAZOP study might resemble the hazard identification (HAZID) process, which is a part of the risk analysis process. However, the term HAZID is often used for purely qualitative risk analyses [56].

When performing a HAZOP study, guide words are used to search for deviations in the intended design (Fig. 6.3). These guidewords are included in the tables to give an impression of the type of deviations that are encountered in the studies.

Guidewords	Interpretation
No	This is a complete negation of the design intention. No part of the intention is achieved and nothing else happens.
More	This is a quantitative increase.
Less	This is a quantitative decrease.
As well as	All the design intention is achieved together with additions.
Part of	Only some of the design intention is achieved.
Reverse	The logical opposite of the intention is achieved.
Other than	Complete substitution, where no part of the original intention is achieved but something quite different happens.
Early	Something happens earlier than expected relative to clock time.
Late	Something happens later than expected relative to clock time.
Before	Something happens before it is expected, relating to order or sequence.
After	Something happens after it is expected, relating to order or sequence.

Fig. 6.3. HAZOP guide words. Adapted from [58]

A HAZOP study is performed for each phase of the lift, i.e., lift-off and in-air manoeuvring (LO), splash-zone crossing (SC), deeply submerged (DS), and landing (LG). Even though there are hazards with negligible risk, measures may be implemented. According to the ALARP principle (section 6.2), low-cost and low-effort measures should be implemented regardless of initial risk.

6.4 HAZOP studies

In this section, I present the findings from the HAZOP studies. The results are presented in Table 6.4-6.7. Each hazard is given an identification in the first column. In the next column, the guide word is placed. This gives us an idea of what causes the deviation. In the fourth column, the possible causes are listed. In the next column, we see the potential consequences of the deviation.

The consequence of several of the hazards is damage to assets. This includes damage to the crane vessel, ITS, ROVs, other equipment and near subsea infrastructure. If subsea infrastructure were to be hit by dropped objects, it could lead to disaster. Damage to, for instance, producing wells or flowlines could cause leakage of hydrocarbons, which could lead to extreme dangers such as explosions and suffocation. However, in this work, it is assumed that the lifting operation takes place far from producing equipment. It is, nevertheless, common practice to shut down production if there is a significant risk of hydrocarbon leakage.

In the sixth, seventh and eighth column, the initial risk of the hazard is estimated.

The column after the initial risk contains required actions to mitigate the risk. All risks above the pre-defined limits should be addressed with a risk-reducing measure. According to the ALARP principle, even negligible risk could have risk-reducing measures.

In the three columns for the reduced risk, we see how the risk-reducing actions have affected the risk. The actions are then allocated to a responsible. This is done to ensure that there is no confusion about who is obligated to implement the action. The last column is dedicated to comments.

Table 6.4 HAZOP study of the lift-off and in-air-manoeuving phase.

Identificat ion	Guide word	Deviation	Possible cause	Consequences	Initial risk			Actions required	Reduced risk			Action allocated to	Comments
					Likelihood	Impact	Risk		Likelihood	Impact	Risk		
LO-1	LESS	Sliding of ITS. Insufficient friction between ITS and deck.	Seafastening removed prematurely. Chemical spill on deck.	Damage to assets and/or personnel.	3	E	75	Do not remove seafastening before permission from supervisor is granted. Inspect deck.	1	E	20	Deck foreman	The seafastening brackets or other barriers can be used as bumpers to prevent vertical motion during lift-off.
LO-2	AFTER	Personnel on deck hit by ITS.	Deck not cleared and closed.	Loss of life. Personnel injury.	2	E	50	Confirm all personnel is out of lifting zone. Appoint responsible for closing off deck.	1	E	20	Deck foreman	Surveil lifting zone if necessary
LO-3	MORE	Failure in lift rigging.	Seafastening not properly removed. Excessive tension in lift rigging. Lifting points on ITS rusty.	Sudden and unexpected movement of subsea ITS that causes collision with deck and/or danger to personnel. Loss of ITS.	2	E	50	Crane and lifting equipment certified and inspected. Check the lift rigging for entanglements and damage, confirm seafastening is removed and communicate clearly with supervisor. Position vessel such that dropped objects do not hit subsea infrastructure.	1	E	20	Shift supervisor	
LO-4	MORE	Excessive crane-tip motion. Sudden crane-vessel motion.	Re-hit when lifted. Slack wire.	Damage to assets and/or personnel. Loss of ITS.	3	D	50	Monitor weather conditions and obtain weather forecasts from different sources. Wind, waves and current are all important. Contract weather expert/meteorologist.	2	C	10	Project engineer	
LO-5	MORE	Pendulum swinging motion of ITS.	Resonance motion of subsea ITS due to vessel motion.	Danger to asset and personnel.	4	C	50	Perform numerical simulations and use tugger lines to prevent vertical motion. Ensure the vessel in facing the correct direction. Survey transit route prior to launch.	2	C	10	Project engineer	Analysis of dynamic response of lifted object.
LO-6	MORE	ITS rotates.	Tugger lines not correctly operated. Tugger line failure.	Danger to asset and personnel.	2	C	10	The use of tugger line depends on the weather conditions.	1	C	5	Shift supervisor	Prone to misjudgement.
LO-7	AFTER	Dropped object.	Loose objects on ITS not removed before operation.	Damage to assets. Retrieval operation could be required.	3	C	25	Inspect ITS before operation. Ensure seafastening is completely removed. Position vessel such that dropped objects do not hit subsea infrastructure.	2	C	10	Shift supervisor	

Table 6.5. HAZOP study of the splash-zone-crossing phase.

Identificat ion	Guide word	Deviation	Possible cause	Consequences	Initial risk			Actions required	Reduced risk			Action allocated to	Comments
					Likelihood	Impact	Risk		Likeliho od	Impact	Risk		
SC-1	MORE	Failure in lift rigging. Excessive tension in lift rigging.	Incorrect judgement of weather. Unexpected wave. Shielding effect not properly accounted for. Suction-anchor ventilation holes not opened. Large dynamic loads.	Damage to assets and/or personnel. Loss of or damage to template. Retrieval operation required.	2	D	25	Perform numerical simulations to find weather window. Inspect ventilation holes prior to operation.	1	D	10	Project engineer and shift supervisor	
SC-2	MORE	Failure in lift rigging.	Excessive vertical motion in template. Slack wire and snap load on lift rigging.	Damage to assets and/or personnel. Loss of or damage to template. Retrieval operation required.	1	D	10	Limit velocity through splash zone. Use numerical simulation to find most critical moment.	1	D	10	Shift supervisor	Project engineer responsible for numerical simulations
SC-3	MORE	Damage to template.	Excessive slamming loads on structure.	Damage to template. Retrieval operation required.	4	C	50	Perform numerical simulations. Change template design if necessary.	2	C	10	Project engineer	

Table 6.6. HAZOP study of the deeply-submerged phase.

Identification	Guide word	Deviation	Possible cause	Consequences	Initial risk			Actions required	Reduced risk			Action allocated to	Comments
					Likelihood	Impact	Risk		Likelihood	Impact	Risk		
DS-1	MORE	Lift rigging snap.	Excessive tension in rigging setup due to vertical resonance. Slack wire and snap load.	Damage to assets and/or personnel. Loss of or damage to template. Retrieval operation required.	2	E	50	Examine weather conditions.	1	E	20	Project engineer	
DS-2	MORE	Incorrect orientation of template	Lift rigging entanglement due to excessive template motion. Unexpected dynamic response and current load.	Operation aborted or delayed.	2	E	50	Visual inspection by ROV during lowering.	1	E	20	ROV team manager	
DS-3	LESS	Collapse of structural members.	Pressure difference in members.	Damage to assets. Retrieval operation required.	3	E	75	Allow the air to escape the suction anchors. Stop the lowering when the template is fully submerged to allow free flooding of structure and equalising of pressure. Use ROV to inspect and open valves if necessary.	1	E	20	Project engineer	
DS-4	NO	ROV collision with tugger lines.	Loss of power to ROV. Current load not accounted for.	Retrieval operation for ROV. Delay.	2	D	25	Clear indications on where to cut tugger lines.	1	D	10	Shift supervisor	
DS-5	NO	Vessel drift off.	DP system failure.	Collision. Damage to assets.	3	D	50	Evaluate reliability of DP system. Stop production in nearby infrastructure. Contract DP system engineer for the operation.	1	D	25	Offshore manager	

Table 6.7. HAZOP study of the landing phase.

Identification	Guide word	Deviation	Possible cause	Consequences	Initial risk			Actions required	Reduced risk			Action allocated to	Comments
					Likelihood	Impact	Risk		Likelihood	Impact	Risk		
LG-1	MORE	Failure in lift rigging.	Slack wire and snap load during touchdown.	Damage to assets and/or personnel. Loss of or damage to ITS. Retrieval operation required.	1	E	20	Limit velocity during landing. Activate the active heave compensator. Monitor operation using ROV.	1	E	20	Shift supervisor	
LG-2	NO	Vessel drift off.	DP system failure. Power generation failure.	Collision. Damage to assets.	3	D	50	Evaluate reliability of DP system. Stop production in nearby infrastructure. Contract DP system engineer for the operation.	1	D	10	Offshore manager	
LG-3	OTHER THAN	Offset from intended position.	Current load.	Time-consuming landing process.	5	D	150	ROV connects tugger lines from ITS to pre-installed clump weights. Tugger lines are used to position ITS correctly.	1	D	10	Shift supervisor	
LG-4	OTHER THAN	Uneven self-penetration.	Unexpected or unfavourable soil conditions.	Misalignment with the rest of the SPS. Retrieval operation required.	5	E	300	Perform levelling procedure. ROV closes ventilation hatches on one or more suction anchors.	1	E	20	ROV team manager	
LG-5	OTHER THAN	Insufficient self-penetration	Unexpected or unfavourable soil conditions.	Misalignment with the rest of the SPS. Retrieval operation required.	4	E	150	Perform suction procedure. ROV connects suction pump to suction anchors.	1	E	20	ROV team manager	
LG-6	OTHER THAN	Excessive self-penetration.	Unexpected or unfavourable soil conditions.	Misalignment with the rest of the SPS. Retrieval operation required.	4	E	150	Perform settling procedure. Hold ITS in position and close ventilation hatches.	1	E	20	ROV team manager	
LG-7	OTHER THAN	Excessive deflection in ITS.	Unexpected or unfavourable soil conditions.	Damage to ITS. Retrieval operation required.	3	E	75	Limit lowering velocity if the limit for allowable deflection is exceeded.	1	E	20	Shift supervisor	Load cells are mounted on the ITS and the signal is transferred to the ROV.

We see from the HAZOP studies that the risks have been successfully reduced for all the hazards. For LO-6, even an acceptably low risk has been reduced. The guide words give us a clear indication of what causes the deviation and the underlying function of it.

For the lift-off and in-air manoeuvring, 5/7 of the deviations are caused by either a quantitative decrease or increase. The remaining two are related to the order of operations.

The splash-zone-crossing zone exhibits only quantitative increase as causes. These are all related to the loads.

For the phase during which the ITS is deeply submerged, the causes are related to quantity as well as a negation of the intended design. One might think that this process is straightforward, but we see from the table that there are risks in need of mitigation.

In contrast to the other phases, we see that 5/7 deviations are caused by a substitution of the intended design for the landing phase. All these hazards carry high risk. The hazard with the highest risk, LG-5, is encountered during this phase. The landing of the template involves a lot of uncertainty. The process of landing the template can be cumbersome process. It must be controlled from the surface, often several hundred meters above the seabed. Not only is it far away, but it also depends on the cooperation between the crane operator, ROV team and the supervisor.

7 Conclusions and further work

With the current situation in the oil and gas industry and all the activity expected in other sectors such as renewable energies and CCS, the need for marine lifting operations on the NCS will remain significant for years to come. Numerical and risk analyses are essential to safely and cost-effectively conduct marine lifting operations.

7.1 Numerical analysis conclusion

The numerical simulations showed that the geometry of the suction anchors affects the lifting-wire tension and thus affects the operability. The Gumbel probability papers showed that the lifting-wire tension decreased with increasing mean zero up-crossing period. Therefore, it is reasonable to assume that other sea states with a mean zero up-crossing period in the region of 4 s will also cause too high tension on the lifting wire.

As no simulations produced lifting-wire tensions close to the lower load limit, it is safe to say that slack wire is unlikely to occur.

7.2 Risk analysis conclusion

From the HAZOP studies, we can see that the guideword MORE is the most prevalent in the lift-off- and in-air-maneuvring phases and the splash-zone-crossing phase. MORE is related to excessive tension, loads and motion. In other words, the majority of the hazards are determined by the geometry, mass and design of the ITS. The weather conditions can potentially affect all the motions related to these hazards. Therefore, the two first phases of a marine lifting operation depend significantly on the weather conditions.

The deeply-submerged phase exhibits significant risks, particularly in comparison with the splash-zone crossing. Similarly, the landing phase involves perhaps a surprisingly high number of potential threats. Misalignment with the SPS is a critical consequence. The operation has to be carefully planned and coordinated.

7.3 Recommendations for future work

Increasing the number of seeds will ensure higher accuracy of the results. The fact that two of the lifting-wire-tension maxima for the mean zero up-crossing period of 4 s were remarkably higher than the rest illustrates the importance of data. If the sea state in those simulations were encountered in an actual lifting operation, it could have led to disaster.

Another point worthy of more attention is the modelling of the hydrodynamic forces. The OrcaFlex model in this work had the coefficients for added mass and slamming assigned to line elements. This could be compared to other ways of modelling them.

Concerning the risk assessment, the transport from the fabrication site could also be included to have a complete picture of the risk of the installation process. Furthermore, other types of studies could be applied to compare the results.

8 References

- [1] Ministry of Petroleum and Energy, *Facts 2014: The Norwegian Petroleum Sector*, 2014. [Online]. Available: https://www.regjeringen.no/globalassets/upload/oed/pdf_filer_2/faktaheftet/fakta2014og/facts_2014_nett_.pdf.
- [2] Norwegian Ministry of Labour and Social Affairs, "Meld.st.12 (2017–2018), Report to the Storting (White paper): Health, Safety and Environment in the petroleum industry," 2018. Accessed: May 28, 2022. [Online]. Available: <https://www.regjeringen.no/contentassets/258cadcb3cca4e3c87c858fd787e0f75/en-gb/pdfs/stm201720180012000engpdfs.pdf//>
- [3] International Energy Agency, "Global Energy Review 2021," Apr. 2021. Accessed: May 18, 2022. [Online]. Available: <https://www.iea.org/reports/global-energy-review-2021>
- [4] International Energy Agency, "World Energy Outlook 2021," Oct. 2021. Accessed: May 18, 2022. [Online]. Available: <https://www.iea.org/reports/world-energy-outlook-2021>
- [5] Norwegian Petroleum. "Production forecasts." <https://www.norskpetroleum.no/en/production-and-exports/production-forecasts//> (accessed May 28, 2022).
- [6] J. A. Pratt, T. Priest, and C. J. Castaneda, *Offshore pioneers: Brown & Root and the history of offshore oil and gas*. Burlington: Gulf Professional Publishing, 1997.
- [7] P. A. Nilsen, "Subsea Technology Enabling Cost Effective Developments – Subsea History and Perspective of the Subsea Future," in *SPE Annual Caspian Technical Conference & Exhibition*, Nov. 4 2015, doi: <https://doi.org/10.2118/177365-ms>.
- [8] Alchetron. "Ormen Lange (gas field)." [https://alchetron.com/Ormen-Lange-\(gas-field\)](https://alchetron.com/Ormen-Lange-(gas-field)) (accessed May 22, 2022).
- [9] Y. Bai and Q. Bai, *Subsea Engineering Handbook*, 2nd ed. Gulf Professional Publishing, 2018.
- [10] D. Devegowda and S. L. Scott, "An Assessment of Subsea Production Systems," in *SPE Annual Technical Conference and Exhibition*, Oct. 2003, vol. All Days, SPE-84045-MS, doi: <https://doi.org/10.2118/84045-ms>.
- [11] Y. Xing and L. Reinås, "OFF550 Subsea Technology," University of Stavanger, Lecture Notes, 2021.
- [12] OneSubsea. "Vertical Dual-Bore Subsea Tree System." <https://www.onesubsea.slb.com/subsea-production-systems/subsea-tree-systems/vertical-dual-bore-subsea-tree-system> (accessed June 3, 2022).
- [13] M. Jansen, C. Duffy, T. C. Green, and I. Staffell, "Island in the Sea: The prospects and impacts of an offshore wind power hub in the North Sea," *Advances in Applied Energy*, vol. 6, p. 100090, June 2022, doi: <https://doi.org/10.1016/j.adapen.2022.100090>.
- [14] L. I. Fendt, Maria, "Why did the IPCC choose 2° C as the goal for limiting global warming?," *Ask MIT Climate*. [Online]. Available: <https://climate.mit.edu/ask-mit/why-did-ipcc-choose-2deg-c-goal-limiting-global-warming>
- [15] C. Benjaminsen, "This is what you need to know about CCS – Carbon Capture and Storage," *Norwegian SciTech News: Research News from NTNU and SINTEF*. [Online]. Available: <https://norwegianscitechnews.com/2019/10/this-is-what-you-need-to-know-about-ccs-carbon-capture-and-storage/>
- [16] Olje- og energidepartementet. "Langskip-prosjektet er i gang." <https://langskip.regjeringen.no/> (accessed June 6, 2022).

- [17] Y. Xing, O. Gaidai, Y. Ma, A. Naess, and F. Wang, "A novel design approach for estimation of extreme responses of a subsea shuttle tanker hovering in ocean current considering aft thruster failure," *Applied Ocean Research*, vol. 123, p. 103179, June 2022, doi: <https://doi.org/10.1016/j.apor.2022.103179>.
- [18] E. Maslin, "Subsea Mining: All Eyes on Marine Minerals Offshore Norway," *MarineLink*. [Online]. Available: <https://www.marinelink.com/news/subsea-mining-eyes-marine-minerals-489614>
- [19] Rystad Energy, "Marine Minerals: Norwegian Value Creation Potential," Nov. 20 2020. Accessed: June 3, 2022. [Online]. Available: <https://norskoljeoggass.no/contentassets/f7a40b81236149ea898b87ff2e43a0e3/20201120-marine-minerals---norwegian-value-creation-potential.pdf>
- [20] H. Reid, "Google, BMW, AB Volvo, Samsung back environmental call for pause on deep-sea mining," *Reuters*. [Online]. Available: <https://www.reuters.com/business/sustainable-business/google-bmw-volvo-samsung-sdi-sign-up-wwf-call-temporary-ban-deep-sea-mining-2021-03-31/>
- [21] D. Denney. "Who Dat Project—Deepwater Subsea Production of Light and Heavy Oil." <https://jpt.spe.org/who-dat-projectdeepwater-subsea-production-light-and-heavy-oil> (accessed June 6, 2022).
- [22] N. O. Hauge and L. Li, "Numerical study on splash zone crossing with subsea template and ROV," University of Stavanger, 2021.
- [23] Wintershall Dea Norge. "Maria: From Discovery to Production." <https://wintershalldea.no/en/where-we-are/maria> (accessed May 23, 2022).
- [24] A. M. N rstad, "Suction Anchor Penetration-Estimating Penetration Resistance Based on CPT Sleeve Friction," Norwegian University of Science and Technology, 2017.
- [25] *Marine Operations and Marine Warranty*, DNV GL, 2016.
- [26] R. B. Tommasini, L. d. O. Carvalho, and R. Pavanello, "A dynamic model to evaluate the influence of the laying or retrieval speed on the installation and recovery of subsea equipment," *Applied Ocean Research*, vol. 77, pp. 34-44, Aug. 2018, doi: <https://doi.org/10.1016/j.apor.2018.05.001>.
- [27] *Modelling and Analysis of Marine Operations*, DNV, 2011.
- [28] *Environmental conditions and environmental loads*, DNV, 2007.
- [29] O. T. Gudmestad, *Marine technology and operations : theory & practice*. Southampton: WIT Press, 2015.
- [30] S. Haver, *Metocean Modelling and Prediction of Extremes*. Stavanger: Haver & havet, University of Stavanger, Norwegian University of Science and Technology, 2018.
- [31] D. E. Newland, *An introduction to random vibrations, spectral and wavelet analysis*, 3rd ed. Harlow: Longman, 1993.
- [32] J. Odland, *OFF515 Offshore Field Development Compendium*. University of Stavanger, 2013.
- [33] Y. Tanaka, "Active vibration compensator on moving vessel by hydraulic parallel mechanism," *International Journal of Hydromechatronics*, vol. 1, p. 350, Jan. 2018, doi: <https://doi.org/10.1504/IJHM.2018.094887>.
- [34] C. Obhrai, "OFF580 Marine Technology and Design," University of Stavanger, Lecture Notes, 2021.
- [35] L. Li, "OFF600 Marine Operations," University of Stavanger, Lecture Notes, 2021.
- [36] L. Li, Z. Gao, and T. Moan, "Response Analysis of a Nonstationary Lowering Operation for an Offshore Wind Turbine Monopile Substructure," *Journal of offshore mechanics*

- and Arctic engineering*, vol. 137, no. 5, p. 51902, Oct. 2015, doi: <https://doi.org/10.1115/1.4030871>.
- [37] L. Li, "OFF600/605 Marine Operations," University of Stavanger, Recorded Lectures, 2020.
- [38] M. Morandau, R. T. Walker, R. Argall, and R. F. Nicholls-Lee, "Optimisation of marine energy installation operations," *International Journal of Marine Energy*, vol. 3-4, pp. 14-26, Dec. 2013, doi: <https://doi.org/10.1016/j.ijome.2013.11.002>.
- [39] L. Li, "OFF585 Engineering Mathematics and Dynamics: Statistical Methods in Marine Technology," University of Stavanger, Lecture Notes, 2020.
- [40] A. Amer, L. Li, and X. Zhu, "Numerical study on the deployment of a subsea template," University of Stavanger, 2020.
- [41] Orcina. "WebHelp." <https://www.orcina.com/webhelp/OrcaFlex/Default.htm> (accessed May 10, 2022).
- [42] P. Fu, B. J. Leira, and D. Myrhaug, "Assessment of Methods for Short-Term Extreme Value Analysis of Riser Collision," Sep. 25 2018, doi: <https://doi.org/10.1115/OMAE2018-78318>.
- [43] T. Aven, *Risk, surprises and black swans : fundamental ideas and concepts in risk assessment and risk management*, New York: Routledge, 2014.
- [44] *Risk management in marine - and subsea operations*, DNV, 2003.
- [45] Standards Norway, *Norsok Standard : Risk and emergency preparedness assessment : Z-013*, 3rd ed. (Risk and emergency preparedness assessment). Lysaker: Standard Norge, 2010.
- [46] O. T. Gudmestad, "Risk Assessment Tools for Use During Fabrication of Offshore Structures and in Marine Operations Projects," *Journal of offshore mechanics and Arctic engineering*, vol. 124, no. 3, pp. 153-161, Aug. 2002, doi: <https://doi.org/10.1115/1.1492825>.
- [47] M. Ibrion, N. Paltrinieri, and A. R. Nejad, "Learning from failures: Accidents of marine structures on Norwegian continental shelf over 40 years time period," *Engineering Failure Analysis*, vol. 111, p. 104487, Apr. 2020, doi: <https://doi.org/10.1016/j.engfailanal.2020.104487>.
- [48] M. Rausand, *Risk Assessment: Theory, Methods, and Applications* (Statistics in practice). Somerset: John Wiley & Sons, Incorporated, 2011.
- [49] T. Aven and J. E. Vinnem, "On the use of risk acceptance criteria in the offshore oil and gas industry," *Reliability Engineering & System Safety*, vol. 90, no. 1, pp. 15-24, Oct. 2005, doi: <https://doi.org/10.1016/j.res.2004.10.009>.
- [50] E. B. Abrahamsen and T. Aven, "Why risk acceptance criteria need to be defined by the authorities and not the industry?," *Reliability Engineering & System Safety*, vol. 105, pp. 47-50, Sep. 2012, doi: <https://doi.org/10.1016/j.res.2011.11.004>.
- [51] T. Aven and Aven, *Risk Analysis: Assessing Uncertainties Beyond Expected Values and Probabilities*, 1st ed. New York: John Wiley & Sons, Incorporated, 2008.
- [52] T. Aven and J. E. Vinnem, *Risk management : with applications from the offshore petroleum industry* (Springer series in reliability engineering). London: Springer, 2007.
- [53] R. Cox, "Risk Assessment and Planning for Offshore Oil Spill Response Preparedness," Mar. 2014, doi: <https://doi.org/10.2118/168336-MS>.
- [54] E. Dudek, K. Krzykowska-Piotrowska, and M. Siergiejczyk, "Risk management in (air) transport with exemplary risk analysis based on the tolerability matrix," *Transport*

- Problems*, vol. 15, pp. 143-156, June 2020, doi: <https://doi.org/10.21307/tp-2020-027>.
- [55] T. Bjerga and T. Aven, "Adaptive risk management using new risk perspectives – an example from the oil and gas industry," *Reliability engineering & system safety*, vol. 134, pp. 75-82, Oct. 2014, doi: <https://doi.org/10.1016/j.ress.2014.10.013>.
- [56] Proactima AS. Online risk-analysis course: Eksempel på risikoanalyse ved løfteoperasjon. (June, 2022).
- [57] Norsk elektroteknisk komite (International Electrotechnical Commission), *Hazard and operability studies (HAZOP studies) : Application guide*, 2nd ed. (Études de danger et d'exploitabilité (études HAZOP) guide d'application). Oslo: Norsk Elektroteknisk komite, 2016.
- [58] H. Lhannaoui, M. I. Kabbaj, and Z. Bakkoury, "Towards an approach to improve business process models using risk management techniques," May, 2013.

9 Appendix A: Spreadsheet containing calculation of hydrodynamic coefficients

9.1 Template A

Calculations according to DNV-RP-H103

Suction-anchor specifications (template A)

Outer diameter, OD	6	m
Inner diameter, ID	5.96	m
Skirt wall thickness, t_s	0.02	m
Height, h	7.9	m
Top plate thickness, t_t	0.03	m
Ventilation-hole diameter, D_v	1	m
Number of ventilation holes, N_v	2	
Steel density, ρ_s	7850	kg/kg ³
Skirt volume, V_s	2.97	m ³
Skirt mass, m_s	23301.17	kg
Top-plate volume, V_t	0.85	m ³
Top-plate mass, m_t	6658.61	kg
Suction anchor mass, m_{tot}	29959.78	kg
Suction anchor mass, m_{tot}	29.96	tonnes

Added-mass calculations

Horizontal added mass

Length-to-diameter ratio, $b/2a$

1.316666667

Interpolate to find added-mass coefficient, C_A

$b/2a$	C_A
1.20	0.62
1.317	0.634
2.50	0.78

Added-mass coefficient, C_A

0.637

Reference volume, V_R

113.10 m³

Water density, ρ_w

1025 kg/m³

Vertical added mass for disc, A_{330}

73800 kg

Horizontal projected area, A_P

28.27 m²

Simplification parameter, λ

0.402

Simplified vertical added mass for disc, A_{33s}

118122.97 kg

Ventilation hole area, A_v

1.57 m³

Perforation rate, p

5.56 %

Vertical added mass with perforation effect, A_{33}

118076.29 kg

Vertical added mass with perforation effect, A_{33}

118.08 tonnes

Vertical added mass due to trapped water

Added mass of trapped water, A_t

225051.03 kg

Added mass of trapped water, A_t

225.05 tonnes

Line elements

Centroid of upper hemisphere, relative to top plate, h_u

1.273 m

Centroid of trapped water, relative to top plate, h_t	3.965	
Centroid of lower hemisphere, relative to top plate, h_l	9.173	m
Upper-hemisphere line-element diameter, D_u	2.546	m
Trapped-water line-element diameter, D_t	1	m
Lower-hemisphere line-element diameter, D_l	1	m
Line-element length for all added-mass line elements, l	1	m
Water density, ρ_w	1025	kg/m ³
Displaced water by upper line element, Δ_u	5220.3	kg
Displaced water by trapped-water line element, Δ_t	805.0	kg
Displaced water by lower line element, Δ_l	805.0	kg

Horizontal drag force

2D steady drag coefficient, $C_{DS,2D}$	1.05	
Height-to-length ratio, L/D	1.316666667	
Reduction factor, κ	0.8	
3D steady drag coefficient, C_{DS}	0.84	
Wave height, H	2	m
Keulegan–Carpenter number, KC	1.047197551	
C_π	1.465714286	
Wake amplification factor for maximum KC number, ψ_{max}	0.465714286	
Drag coefficient, C_D	0.3912	

Mass moment of inertia

Mass moment of inertia in x- and y-direction, I_x, I_y	240325.9617	kg*m ²
Mass moment of inertia in z-direction, I_z	268244.6052	kg*m ²

Normalised submergence for upper line element, $(h/r)_u$	Normalised submergence for trapped-water line element, $(h/r)_t$	Normalised submergence for lower line element, $(h/r)_l$
-1.00	6.93	17.35
-0.99	6.94	17.36
-0.75	7.18	17.60
-0.50	7.43	17.85
-0.25	7.68	18.10
0.00	7.93	18.35
0.25	8.18	18.60
0.50	8.43	18.85
0.75	8.68	19.10
1.00	8.93	19.35
1.25	9.18	19.60
1.50	9.43	19.85
1.75	9.68	20.10
2.00	9.93	20.35

2.25	10.18	20.60
2.50	10.43	20.85
2.75	10.68	21.10
3.00	10.93	21.35
4.00	11.93	22.35
5.00	12.93	23.35

Variable added-mass coefficient for upper line element, C_{Au}	Variable added-mass coefficient for trapped-water line element, C_{At}	Variable added-mass coefficient for lower line element, C_{Al}
0.00	0.00	0.00
0.08	1.96	0.51
1.98	48.92	12.83
3.96	97.84	25.67
4.81	118.81	31.17
5.65	139.78	36.67
5.94	146.77	38.50
6.22	153.76	40.33
6.79	167.73	44.00
7.35	181.71	47.67
8.20	202.68	53.17
9.05	223.64	58.67
9.61	237.62	62.34
10.18	251.60	66.00
10.35	255.79	67.10
10.52	259.99	68.20
10.63	262.78	68.94
10.74	265.58	69.67
10.80	266.98	70.04
10.86	268.37	70.40

Rate of change of added-mass coefficient for upper line element, $dC_{Au}/d(h/r)_u$	Rate of change of added-mass coefficient for trapped-water line element, $dC_{At}/d(h/r)_t$	Rate of change of added-mass coefficient for lower line element, $dC_{Al}/d(h/r)_l$
0.00	0.00	0.00
11.31	279.55	73.34
7.92	195.69	51.34
5.65	139.78	36.67
3.96	97.84	25.67
2.49	61.50	16.13
1.70	41.93	11.00
1.13	27.96	7.33
1.47	36.34	9.53
5.09	125.80	33.00

3.96	97.84	25.67
2.60	64.30	16.87
1.92	47.52	12.47
1.36	33.55	8.80
1.02	25.16	6.60
0.68	16.77	4.40
0.45	11.18	2.93
0.34	8.39	2.20
0.11	2.80	0.73
0.00	0.00	0.00

Negative rate of change of added-mass coefficient for upper line element, $dC_{AU}/d(h/r)_U$	Negative rate of change of added-mass coefficient for trapped-water line element, $dC_{At}/d(h/r)_t$	Negative rate of change of added-mass coefficient for lower line element, $dC_{Al}/d(h/r)_l$
0.00	0.00	0.00
-11.31	-279.55	-73.34
-7.92	-195.69	-51.34
-5.65	-139.78	-36.67
-3.96	-97.84	-25.67
-2.49	-61.50	-16.13
-1.70	-41.93	-11.00
-1.13	-27.96	-7.33
-1.47	-36.34	-9.53
-5.09	-125.80	-33.00
-3.96	-97.84	-25.67
-2.60	-64.30	-16.87
-1.92	-47.52	-12.47
-1.36	-33.55	-8.80
-1.02	-25.16	-6.60
-0.68	-16.77	-4.40
-0.45	-11.18	-2.93
-0.34	-8.39	-2.20
-0.11	-2.80	-0.73
0.00	0.00	0.00

9.2 Template B

Calculations according to DNV-RP-H103

Suction-anchor specifications (template B)

Outer diameter, OD	5.5	m
Inner diameter, ID	5.48	m
Skirt wall thickness, t_s	0.02	m
Height, h	8.225	m
Top plate thickness, t_t	0.03	m
Ventilation-hole diameter, D_v	1	m

Number of ventilation holes, N_v	2	
Steel density, ρ_s	7850	kg/kg ³
Skirt volume, V_s	1.42	m ³
Skirt mass, m_s	11135.96	kg
Top-plate volume, V_t	0.71	m ³
Top-plate mass, m_t	5595.08	kg
Suction anchor mass, m_{tot}	16731.04	kg
Suction anchor mass, m_{tot}	16.73	tonnes

Added-mass calculations

Horizontal added mass

Length-to-diameter ratio, $b/2a$

1.495454545

Interpolate to find added-mass coefficient, C_A

$b/2a$	C_A
1.20	0.62
1.495	0.656
2.50	0.78

Vertical added mass due to top plate

Added-mass coefficient, C_A	0.637	
Reference volume, V_R	87.11	m ³
Water density, ρ_w	1025	kg/m ³
Vertical added mass for disc, A_{330}	56844.79167	kg
Horizontal projected area, A_P	23.76	m ²
Simplification parameter, λ	0.372	
Simplified vertical added mass for disc, A_{33s}	91811.50	kg
Ventilation hole area, A_v	1.57	m ³
Perforation rate, p	6.61	%
Vertical added mass with perforation effect, A_{33}	91506.69	kg
Vertical added mass with perforation effect, A_{33}	91.51	tonnes

Vertical added mass due to trapped water

Added mass of trapped water, A_t	198117.95	kg
Added mass of trapped water, A_t	198.12	tonnes

Line elements

Centroid of upper hemisphere, relative to top plate, h_u	1.167	m
Centroid of trapped water, relative to top plate, h_t	4.128	
Centroid of lower hemisphere, relative to top plate, h_l	9.392	m
Upper-hemisphere line-element diameter, D_u	2.334	m
Trapped-water line-element diameter, D_t	1	m
Lower-hemisphere line-element diameter, D_l	1	m
Line-element length for all added-mass line elements, l	1	m
Water density, ρ_w	1025	kg/m ³
Displaced water by upper line element, Δ_u	4386.5	kg
Displaced water by trapped-water line element, Δ_t	805.0	kg
Displaced water by lower line element, Δ_l	805.0	kg

Horizontal drag force

2D steady drag coefficient, $C_{DS,2D}$	1.05
Height-to-length ratio, L/D	1.495454545
Reduction factor, κ	0.8
3D steady drag coefficient, C_{DS}	0.84
Wave height, H	2 m
Keulegan–Carpenter number, KC	1.142397329
C_{τ}	1.465714286
Wake amplification factor for maximum KC number, ψ_{max}	0.465714286
Drag coefficient, C_D	0.3912

Mass moment of inertia

Mass moment of inertia in x- and y-direction, I_x, I_y	115312.7857	kg*m ²
Mass moment of inertia in z-direction, I_z	126222.8182	kg*m ²

Normalised submergence for upper line element, $(h/r)_u$	Normalised submergence for trapped-water line element, $(h/r)_t$	Normalised submergence for lower line element, $(h/r)_l$
-1.00	7.26	17.78
-0.99	7.27	17.79
-0.75	7.51	18.03
-0.50	7.76	18.28
-0.25	8.01	18.53
0.00	8.26	18.78
0.25	8.51	19.03
0.50	8.76	19.28
0.75	9.01	19.53
1.00	9.26	19.78
1.25	9.51	20.03
1.50	9.76	20.28
1.75	10.01	20.53
2.00	10.26	20.78
2.25	10.51	21.03
2.50	10.76	21.28
2.75	11.01	21.53
3.00	11.26	21.78
4.00	12.26	22.78
5.00	13.26	23.78

Variable added-mass coefficient for upper line element, C_{Au}	Variable added-mass coefficient for upper line element, C_{At}	Variable added-mass coefficient for lower line element, C_{Al}
0.00	0.00	0.00
0.07	1.72	0.40
1.83	43.07	9.95
3.65	86.13	19.89
4.43	104.59	24.15
5.22	123.05	28.42
5.48	129.20	29.84
5.74	135.35	31.26
6.26	147.66	34.10
6.78	159.96	36.94
7.56	178.42	41.20
8.34	196.88	45.47
8.87	209.18	48.31
9.39	221.49	51.15
9.54	225.18	52.00
9.70	228.87	52.86
9.80	231.33	53.42
9.91	233.79	53.99
9.96	235.02	54.28
10.01	236.26	54.56

Rate of change of added-mass coefficient for upper line element, $dC_{Au}/d(h/r)_u$	Rate of change of added-mass coefficient for trapped-water line element, $dC_{At}/d(h/r)_t$	Rate of change of added-mass coefficient for lower line element, $dC_{Al}/d(h/r)_l$
0.00	0.00	0.00
10.43	246.10	56.83
7.30	172.27	39.78
5.22	123.05	28.42
3.65	86.13	19.89
2.29	54.14	12.50
1.56	36.91	8.53
1.04	24.61	5.68
1.36	31.99	7.39
4.69	110.74	25.58
3.65	86.13	19.89
2.40	56.60	13.07
1.77	41.84	9.66
1.25	29.53	6.82
0.94	22.15	5.12
0.63	14.77	3.41
0.42	9.84	2.27

0.31	7.38	1.71
0.10	2.46	0.57
0.00	0.00	0.00

Negative rate of change of added-mass coefficient for upper line element, $dCA_u/d(h/r)_u$	Negative rate of change of added-mass coefficient for trapped-water line element, $dCA_t/d(h/r)_t$	Negative rate of change of added-mass coefficient for lower line element, $dCA_l/d(h/r)_l$
0.00	0.00	0.00
-10.43	-246.10	-56.83
-7.30	-172.27	-39.78
-5.22	-123.05	-28.42
-3.65	-86.13	-19.89
-2.29	-54.14	-12.50
-1.56	-36.91	-8.53
-1.04	-24.61	-5.68
-1.36	-31.99	-7.39
-4.69	-110.74	-25.58
-3.65	-86.13	-19.89
-2.40	-56.60	-13.07
-1.77	-41.84	-9.66
-1.25	-29.53	-6.82
-0.94	-22.15	-5.12
-0.63	-14.77	-3.41
-0.42	-9.84	-2.27
-0.31	-7.38	-1.71
-0.10	-2.46	-0.57
0.00	0.00	0.00

10 Appendix B: MATLAB code for post-processing of results

```
% Martin Lervik 01.12.2021
% Student 249280
close all
clear all

%% Data loading from excel file
A(:,:,1) = xlsread('A-Dynamic hook load',1); % Template A, no waves
A(:,:,2) = xlsread('A-Dynamic hook load',2); % Template A, Tz = 4
A(:,:,3) = xlsread('A-Dynamic hook load',3);
A(:,:,4) = xlsread('A-Dynamic hook load',4);
A(:,:,5) = xlsread('A-Dynamic hook load',5);

B(:,:,1) = xlsread('B-Dynamic hook load',1);
B(:,:,2) = xlsread('B-Dynamic hook load',2);
B(:,:,3) = xlsread('B-Dynamic hook load',3);
B(:,:,4) = xlsread('B-Dynamic hook load',4);
B(:,:,5) = xlsread('B-Dynamic hook load',5);

%% Find seeds with maximum values
M = A(:,:,1);
t = M(651:end,1); % Time column from 0 seconds
n = 1:5; % Number of periods simulated
timeA = zeros(numel(n),1);
seedA = timeA;
for i=n
    M = A(:,:,i);
    M = M(651:end,2:end); % To omit the seconds before sim starts and
time column
    A_red(:,:,i) = M; % Stock reduced data
    [max_val, max_idx]=max(M(:));
    [time,seed]=ind2sub(size(M),find(M==max_val)); % Find seed with
highest values
    timeA(i) = time(1); % In case there are multiple maxima
    seedA(i) = seed(1);
    Amax(i) = max_val; % Stock maximum for each Tz
end

timeB = zeros(numel(n),1);
seedB = timeB;
for i=n
    M = B(:,:,i);
    M = M(651:end,2:end); % To omit the seconds before sim starts and
time column
    B_red(:,:,i) = M;
    [max_val, max_idx]=max(M(:));
    [time,seed]=ind2sub(size(M),find(M==max_val)); % Find seed (column)
with highest values
    timeB(i) = time(1); % In case there are multiple maxima
    seedB(i) = seed(1);
    Bmax(i) = max_val; % Stock maximum for each Tz
end

A1 = A_red(:,:,1); % Template A, no waves
A2 = A_red(:,:,2); % Template A, Tz = 4 s
A3 = A_red(:,:,3);
A4 = A_red(:,:,4);
A5 = A_red(:,:,5);

B1 = B_red(:,:,1);
```

```

B2 = B_red(:,:,2);
B3 = B_red(:,:,3);
B4 = B_red(:,:,4);
B5 = B_red(:,:,5);

%% Plotting scenarios with maximum values
figure
plot(t, A2(:,seedA(2))), xlabel('Time (s)'),ylabel('Load (kN)'),
title('Lifting-wire tension, Template A, Tz = 4 s, Seed 6')
figure
plot(t, B2(:,seedB(2))), xlabel('Time (s)'),ylabel('Load (kN)'),
title('Lifting-wire tension, Template B, Tz = 4 s, Seed 6')

%% Plotting no wave and Tz = 4, B
figure
plot(t, B1(:,seedB(1))), xlabel('Time (s)'),ylabel('Load (kN)'),
title('Lifting-wire tension, Template B')
hold on
plot(t, B2(:,seedB(5)))
legend('No wave','Tz = 4 s')

%% Fitting probability paper, A, All sea states individually
rawsample(1,:) = max(A2);
rawsample(2,:) = max(A3);
rawsample(3,:) = max(A4);
rawsample(4,:) = max(A5);

sample = sort(rawsample,2); % Ordered sample
k=1:length(sample);
n=numel(k);
Fhat=k/(n+1);

% Gumbel probability paper
xg=sample; % x coordinates
yg=-log(-log(Fhat)); % y coordinates

%% Plot Tz = 4s
% Method of moments
sampleaverage=mean(sample(1:,:), 'all'); % Expected value
sampleSTD=sqrt(var(sample(1:))); % Standard deviation

% Gumbel
syms a b % alfa, beta
Ex = a+0.57722*b;
STDx = 1.28255*b;

[a,b]=solve(Ex==sampleaverage, STDx==sampleSTD, a, b);

a=vpa(a); % alfa
b=vpa(b); % beta

figure
plot(xg(1,:),yg,'o'), xlabel('X Gumbel'),ylabel('Y Gumbel'), title('Gumbel
probability paper')
hold on
plot(sample(1,:), (sample(1:)-a)/b)

legend('Tz = 4s','Gumbel fit')

```